THE ASTROPHYSICAL JOURNAL, 449:258–279, 1995 August 10

OPTICAL AND ULTRAVIOLET ANALYSES OF ZZ CETI STARS AND STUDY OF THE ATMOSPHERIC CONVECTIVE EFFICIENCY IN DA WHITE DWARFS

P. BERGERON,[1] F. WESEMAEL, R. LAMONTAGNE,[1] AND G. FONTAINE
Département de Physique, Université de Montréal, C.P. 6128, Succ. Centre-Ville Montréal, Québec, Canada, H3C 3J7;
bergeron, wesemael, lamont, fontaine@astro.umontreal.ca

R. A. SAFFER
Space Telescope Science Institute, 3700 San Martin Drive, Baltimore, MD 21218; saffer@stsci.edu

AND

N. F. ALLARD
Observatoire de Paris-Meudon, Département Atomes et Molécules en Astrophysique; and CNRS Institut d'Astrophysique,
98 bis Boulevard Arago, 75014 Paris, France; allard@iap.fr
Received 1995 January 9; accepted 1995 February 20

ABSTRACT

New high signal-to-noise optical spectrophotometry is presented for 22 ZZ Ceti stars. The atmospheric parameters ($T_{\rm eff}$, log g) and the mass are derived for each object using new model atmospheres and synthetic spectra calculated within the mixing-length theory, as well as recent published mass-radius relationships. Various parameterizations of the convective efficiency are explored. The mass distribution obtained from the optical solutions indicate that the so-called ML2 parameterization of the mixing-length theory yields a mean mass of 0.58 $M_\odot$, in excellent agreement with that of hotter DA stars (0.59 $M_\odot$) whose atmospheres are completely radiative. ML1 and ML3 models, on the other hand, yield mean masses which are, respectively, too high (0.70 $M_\odot$) and too low (0.51 $M_\odot$). With ML2 models, ZZ Ceti stars are found within a narrow instability strip located in the range $13{,}650 \geq T_{\rm eff} \geq 11{,}960$ K.

A similar analysis of *IUE* and *HST* spectroscopic observations is presented as well. It is first shown that a unique solution for $T_{\rm eff}$ and log g cannot be achieved on the basis of ultraviolet spectroscopy alone, and that one of these parameters needs to be constrained independently. When log g values from the optical analysis are adopted, the analysis of the ultraviolet data requires a parameterization less efficient than ML2. Models calculated with ML2/$\alpha = 0.6$ are shown to provide an excellent internal consistency between ultraviolet and optical temperatures. The corresponding instability strip becomes cooler and narrower ($12{,}460 \geq T_{\rm eff} \geq 11{,}160$ K) than that inferred from ML2 models. Furthermore, the atmospheric parameters obtained with these models are consistent with the observed photometry, the trigonometric parallax measurements, and the gravitational redshift masses. However, the mean mass of the sample increases to a value $\sim$0.06 $M_\odot$ larger than that of hotter DA stars. An explanation for this discrepancy is offered in the light of recent nonadiabatic calculations. The overall consistency of our analysis for DA stars outside the ZZ Ceti instability strip is discussed as well.

Subject headings: convection — stars: atmospheres — stars: oscillations — ultraviolet: stars — white dwarfs

1. INTRODUCTION

In the twenty-odd years since their discovery, notable progress has been made in our understanding of the properties of pulsating DA (ZZ Ceti) stars. Key review papers narrating this progress have successively been presented by McGraw (1977), Robinson (1979), Winget & Fontaine (1982), Van Horn (1984), Winget (1988), and Kawaler & Hansen (1989). However, despite the advances reported in these papers, shortcomings in the quality of the observational data and the lack of sufficiently powerful theoretical tools have historically impeded the identification of individual pulsation modes in these stars. Without mode identification, inferences about the internal structure are not possible. Fortunately, the situation is changing rapidly, thanks to observational campaigns such as the Whole Earth Telescope (Nather 1989; Nather et al. 1990; Winget 1991) which provide data of exceptionally high temporal resolution, to observations on large telescopes such as our own ongoing program at the Canada-France-Hawaii Telescope which provide data of unprecedented sensitivity (e.g., Fontaine et al. 1991; Brassard et al. 1993; Bergeron et al. 1993), and to recent advances on the theoretical front including both adiabatic (Brassard et al. 1991; 1992a, b, c; Bradley & Winget 1991; Fontaine et al. 1992) and nonadiabatic studies (Bradley & Winget 1994a; Fontaine et al. 1994; Brassard et al. 1995a).

The task of mode identification in ZZ Ceti stars remains nevertheless complicated because these pulsators show typically only a few excited modes out of the very rich g-mode spectra available to them. This is in contrast to their hot counterparts, the pulsating DB and DO white dwarfs, which generally reveal period spectra containing enough components to be able to build period spacings and period ratios with which to compare to theory. On the basis of their rich observed period spectra, impressive results were obtained in the asteroseismological analyses of the hot pulsating DO white dwarfs PG 1159−035 (Winget et al. 1991; Kawaler & Bradley 1994) and PG 2131+066 (Kawaler et al. 1995), as well as the DB variable GD 358 (Winget et al. 1994; Bradley & Winget

[1] Visiting Astronomer, Cerro-Tololo Inter-American Observatory, National Optical Astronomical Observatories, which is operated by AURA, Inc., under contract with the National Science Foundation.

1994b). As discussed by Brassard, Fontaine, & Wesemael (1995), the scarce period data available for most ZZ Ceti stars preclude a similar approach, and independent constraints on these pulsators must be sought. Brassard, Fontaine, & Wesemael (1995b) suggest exploiting the nonlinear structure observed at very high sensitivity in the Fourier spectra of many of these objects (see also Brickhill 1991, 1992a, b). Model atmosphere analyses of the time-averaged spectra of ZZ Ceti stars constitute other (and sometimes essential) means with which to constrain mode identification by providing *independent* estimates of their atmospheric parameters. This is an avenue which we explore further in the paper.

From an historical perspective, the ZZ Ceti stars are among the most thoroughly studied white dwarfs in the literature, with atmospheric parameters obtained in several independent investigations, with various techniques, and for different regions of the electromagnetic spectrum (see the review by Wesemael et al. 1991). For instance, Weidmann & Koester (1984) have used multichannel spectrophotometer data to determine the atmospheric parameters of a dozen ZZ Ceti stars, while Wesemael et al. (1991) have relied upon the Strömgren photometry of McGraw (1979) and Fontaine et al. (1985) to derive temperatures for a sample of comparable size. Independent estimates have been obtained for a sample of 10 ZZ Ceti stars by Daou et al. (1990) using line profile fitting techniques. Also, ultraviolet (UV) data have been presented and analyzed in several investigations (Wesemael, Lamontagne, & Fontaine 1986; Lamontagne, Wesemael, & Fontaine 1987; Lamontagne et al. 1989; Kepler & Nelan 1993; Koester & Allard 1993; Koester, Allard, & Vauclair 1994). As discussed in detail by Wesemael et al. (1991), even though the boundaries of the ZZ Ceti instability strip inferred from these analyses are generally in good agreement, the effective temperature determinations of individual objects may vary considerably from one analysis to another. Thus, atmospheric parameters of ZZ Ceti stars still remain uncertain, and progress toward a better determination of these parameters can only be accomplished from a simultaneous analysis of the available observing material.

Such an endeavour requires an equally important progress in the modeling of the emergent flux of ZZ Ceti stars. Although the continuous and line opacities in DA stars are fairly well understood, those associated with the H_2^+ and H_2 quasi-molecular absorption features near 1400 and 1600 Å have been studied in detail only recently. For instance, Allard & Koester (1992) have presented new theoretical calculations of these satellite features, and applied their results to a sample of $\sim$40 lukewarm ($20{,}000 \gtrsim T_{\rm eff} \gtrsim 9000$ K) DA stars. These calculations represent a significant improvement over the previous, more approximate treatments of Koester et al. (1985) and Nelan & Wegner (1985). The calculations of these satellite features have been improved even more recently by Allard et al. (1994), where all transitions involved in the H-H and H-H^+ collisions are now taken into account. These latest profiles have been first applied in the context of ZZ Ceti stars by Koester et al. (1994) to determine the atmospheric parameters of G117-B15A from FOS observations with the *Hubble Space Telescope* (*HST*).

Despite these important theoretical improvements, however, the largest uncertainty in our ability to model the emergent spectra of ZZ Ceti stars remains the treatment of convection. Bergeron, Wesemael, & Fontaine (1992b) have shown that the predicted fluxes *at all wavelengths* of models in the ZZ Ceti temperature range depend strongly on the assumed convective efficiency. In particular, the absolute fluxes, line profiles, UV energy distributions, color indices, and equivalent widths are found to be extremely sensitive to the parameterization of the mixing-length theory (MLT) commonly used in model atmosphere calculations. In this paper, we attempt to constrain the convective efficiency in ZZ Ceti stars by comparing new optical and archival UV observations with the predictions of model atmosphere calculations.

2. OPTICAL ANALYSIS

Our earlier efforts to determine the atmospheric parameters of ZZ Ceti stars using optical spectroscopy have been presented in Daou et al. (1990). We first summarize some of the content of that analysis, and justify the reasons for repeating here a more detailed spectroscopic analysis of the ZZ Ceti stars.

2.1. *Daou et al. Analysis*

Daou et al. (1990) presented a spectroscopic analysis of a sample of 10 ZZ Ceti stars, and determined $T_{\rm eff}$ and $\log g$ for all objects using line profile fitting techniques. As discussed by Daou et al., the spectra used in that analysis had been acquired as part of a backup project by various observers, and with different telescopes, spectrographs, detectors, and reduction procedures. As such, their spectroscopic sample is somewhat inhomogeneous, with a signal-to-noise ratio which varies from S/N $\sim$ 20 up to 70 in the best-exposed objects, and with a spectral resolution in the range 3–9 Å FWHM. Furthermore, because of the differences in spectral coverage, the analysis of Daou et al. was restricted to Hγ up to H9, and in some cases, only up to H8 and even Hϵ for G226−29.

The model spectra used by Daou et al. are those described at length in Bergeron, Wesemael, & Fontaine (1991) which include the occupation probability formalism of Hummer & Mihalas (1988). This formalism allows a detailed calculation of the level populations in the presence of perturbations from neighboring particles, and provides as well a consistent description of bound-bound and bound-free transitions. Despite these improvements, the analysis of Daou et al. was not free of complications. Indeed, since ZZ Ceti stars fall close to the temperature range where the equivalent widths of the Balmer lines reach a maximum (see, e.g., Fig. 2 of Daou et al.), some stars had two χ^2 minima in the $T_{\rm eff}$–$\log g$ plane, corresponding to solutions on each side of the maximum of the equivalent widths. While for most objects it was still possible to exclude one of these solutions on the basis of existing photometric observations, some objects retained two acceptable solutions.

Since that analysis, our observational techniques and theoretical models have improved significantly. Both aspects are discussed in the study of the mass distribution of DA white dwarfs by Bergeron, Saffer, & Liebert (1992a, hereafter BSL). There, high signal-to-noise spectroscopy of 129 DA stars has been obtained in a highly homogeneous fashion, and compared with the predictions of model atmospheres. These new models made use of the improved Stark broadening profiles calculated by T. Schöning & K. Butler (1991, private communication) for the complete Balmer line series; the models of Bergeron et al. (1991) employed a much more approximate treatment for Hϵ and higher lines. Moreover, preliminary results of the BSL analysis indicated that systematic differences were found between the atmospheric parameters obtained from individual Balmer lines, an effect which was

traced back to the treatment of line broadening itself. As discussed by Seaton (1990), the individual Stark components of a given line profile become gradually destroyed in the presence of a strong perturbing field, an effect which reduces the line opacity in the regions where the line wings strongly overlap. Bergeron (1993) has shown that this important effect can be reproduced, to some extent, by adjusting the value of the microfield in the Hummer-Mihalas formalism. The predicted line profiles are different enough from those of Bergeron et al. (1991) that a fresh look at the determination of the atmospheric parameters of ZZ Ceti stars using optical spectroscopy seem appropriate.

2.2. *Spectroscopic Observations*

Since it became clear that a step forward in the determination of the atmospheric parameters of ZZ Ceti stars could only be accomplished with a similar improvement in observational data, it was deemed necessary to reacquire optical spectra for the ZZ Ceti stars using the same instrument setup and reduction techniques outlined in BSL and Saffer et al. (1994). We have thus acquired new high signal-to-noise spectroscopic observations for 18 ZZ Ceti stars using the 2.3 m telescope at Steward Observatory, equipped with the Boller & Chivens spectrograph and a Texas Instrument CCD detector (see BSL for additional details). The spectral coverage is $\sim$3750–5100 Å, thus covering Hβ up to H9 at an intermediate resolution of $\sim$6 Å FWHM.

Spectra of four additional ZZ Ceti stars from the southern hemisphere (BPM 31594, BPM 30551, L19-2, and LTT 4816) have also been secured. Even though the spectra are of comparable quality to those obtained at the Steward Observatory, these four stars will be treated separately throughout our analysis to preserve the homogeneity of our spectroscopic sample. The spectrum of LTT 4816 is taken from the spectroscopic analysis of Bragaglia, Renzini, & Bergeron (1995). Although there are nine observations of LTT 4816 in that analysis, here we retain only the best spectrum. The spectra of BPM 31594, BPM 30551, and L19-2 have been obtained with the CTIO 4 m telescope, the RC spectrograph, the Blue Air Schmidt Camera, and the 400 × 1200 Reticon detector. The spectral coverage and resolution are similar to those of the Steward Observatory setup (the spectral resolution of BPM 31594 and LTT 4816 is $\sim$9 Å FWHM).

As in Daou et al., the exposure times were set long enough to cover several pulsation cycles (for an average of $\sim$4.8 cycles) in order to obtain meaningful time-averaged spectra. As such, the signal-to-noise ratio varies considerably from star to star, with an imposed lower limit of $\sim$80, although most spectra have S/N $\gtrsim$ 100. The journal of observations is presented in Table 1, together with the V magnitudes (Johnson V, or when not available, multichannel V), the period of the dominant pulsation mode, and the available trigonometric parallax measurements, used later in our analysis. Our optical spectra for the ZZ Ceti stars are displayed in Figure 1.

2.3. *Atmospheric Parameter Determination*

Our model atmospheres and synthetic spectra are similar to those described in BSL and references therein. Here we simply describe the new physics included in the calculations.

All the opacity sources are taken from the new code of Bergeron, Saumon, & Wesemael (1995) in which continuous absorptions are updated from the work of Lenzuni, Chernoff, & Salpeter (1991). In particular, the H_2^+ bound-free and free-free opacities are found to have a small, but nonnegligible contribution to the total opacity in the ZZ Ceti temperature range. More important, we are now taking into account the opacity from the satellite absorption features of the H_2^+ and H_2 quasi-molecules near 1400 and 1600 Å, first introduced in our calculations using the results published by Allard & Koester (1992). After a preliminary completion of our analysis, Allard et al. (1994) obtained new results in which all the transitions involved, due to H-H and H-H^+ collisions, are taken into consideration. These improved calculations are thus used here. The quasi-molecular opacities not only affect the emergent UV

TABLE 1

JOURNAL OF OBSERVATIONS

WD	Name	Date (UT)	Exposure Time (s)	Period (s)	V	π
0133−116	R548	1990 Oct 10	1200	213	14.16	0".0149 ± 0".0020
0416+272	HL 76	1990 Nov 25	1200	494	15.2	...
0417+361	G38-29	1990 Oct 11	2400	925	15.59	0.0136 ± 0.0041
0455+553	G191-16	1990 Oct 11	3600	883	15.98	...
0517+307	GD 66	1990 Nov 25	1800	271	15.56	...
0858+363	GD 99	1990 Nov 26	1200	260	14.55	...
0921+354	G117-B15A	1991 Mar 8	1800	215	15.50	0.0105 ± 0.0042
1159+803	G255-2	1991 Mar 8	3200	830	16.04	...
1307+354	GD 154	1991 Mar 8	1600	1186	15.33	...
1350+656	G238-53	1991 Mar 8	1900	206	15.51	...
1422+095	GD 165	1991 Mar 8	650	120	14.32	0.0278 ± 0.0034
1559+369	R808	1991 Mar 8	2400	833	14.36	0.0310 ± 0.0035
1647+591	G226-29	1990 Oct 11	600	110	12.24	0.0819 ± 0.0046
1855+338	G207-9	1990 Oct 10	1200	292	14.62	0.0305 ± 0.0044
1935+276	G185-32	1990 Oct 10	600	215	12.97	0.0557 ± 0.0029
1950+250	GD 385	1990 Oct 10	1200	256	15.12	0.0263 ± 0.0032
2303+242	PG 2303+243	1990 Oct 10	1800	578	15.5	...
2326+049	G29-38	1990 Oct 10	1200	615	13.03	0.0734 ± 0.0040
0104−464	BPM 30551	1994 Sep 14	1200	823	15.26	...
0341−459	BPM 31594	1994 Dec 11	1200	617	15.03	...
1236−495	LTT 4816	1988 Jan 20	600	192	13.96	0.0610 ± 0.0094
1425−811	L19-2	1994 Sep 15	900	600	13.75	...

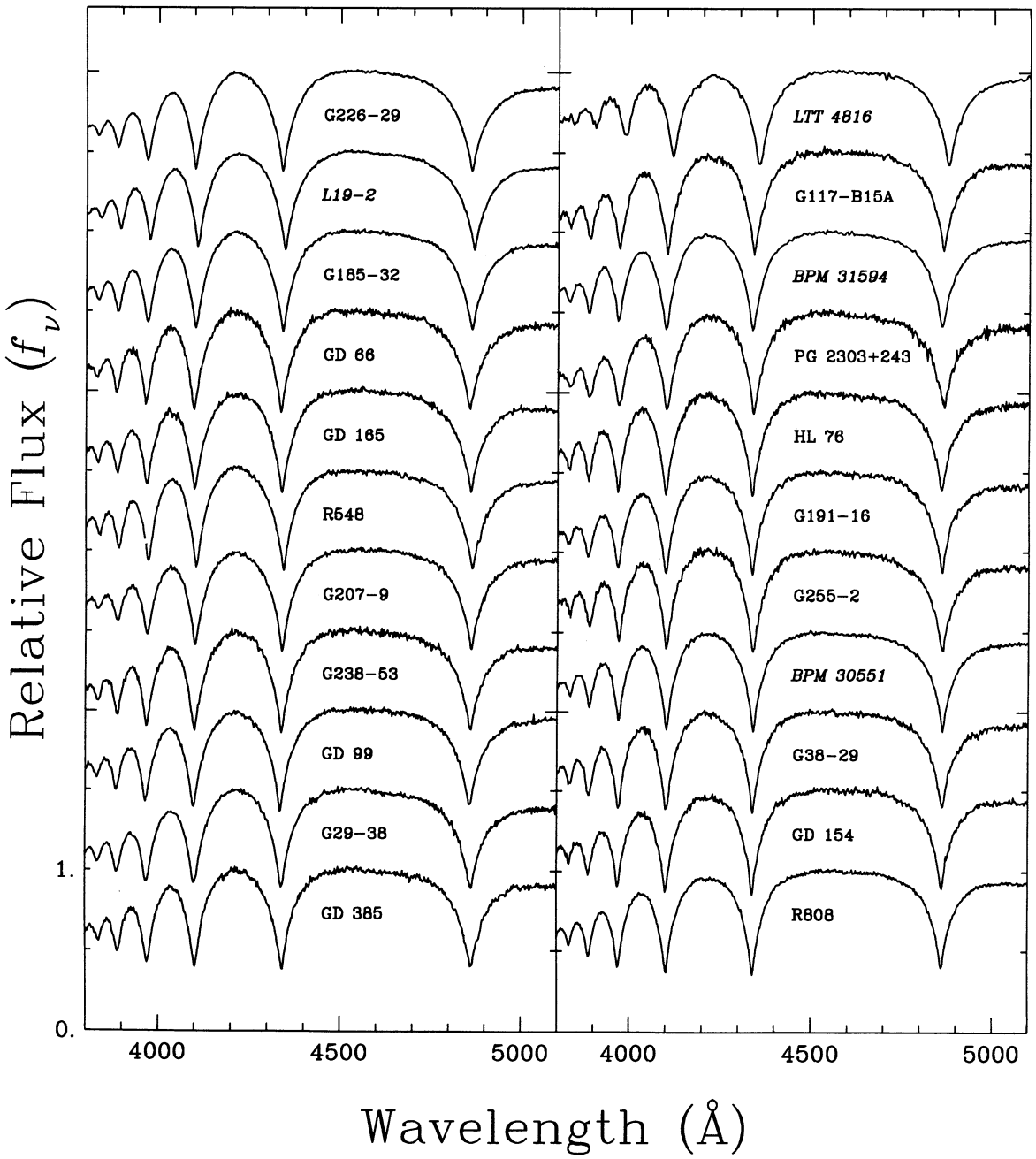

FIG. 1.—Optical spectra for the sample of ZZ stars listed in Table 1. The effective temperatures decrease from upper left to bottom right. The spectra are normalized at 4500 Å and are offset vertically by a factor of 0.5. The names in italics correspond to the four stars at the bottom of Table 1 which have been observed with a different setup than the rest of the sample; these are treated separately in our analysis.

fluxes, but modify the temperature profile of the models as well. Therefore, these opacities need to be included directly in the calculations of the atmospheric structures, as first carried out by Koester & Allard (1993). We note that this latest generation of opacities has also been used by Koester et al. (1994) to model successfully the *HST* observations of G117-B15A.

We consider in the following various parameterizations of the MLT. We make extensive use of the nomenclature first introduced by Fontaine, Villeneuve, & Wilson (1981). The ML1 and ML2 versions correspond to the descriptions of Böhm-Vitense (1958) and Böhm & Cassinelli (1971), respectively. These two versions differ in their definitions of the constants a, b, and c used in the equations for the convective flux (see Bergeron et al. 1992b for details), while both assume a ratio of the mixing length to the pressure scale height of $\alpha \equiv l/H = 1$. The ML2 parameterization reduces the horizontal energy loss rate, increasing the convective efficiency relative to the ML1 version (Tassoul, Fontaine, & Winget 1990). The ML3 version is identical to the ML2 version but with a value of $\alpha = 2$. ML3 models are thus characterized by an even larger convective efficiency than ML2 models. Emergent fluxes with these versions of the MLT have already been presented by

Bergeron et al. (1992b), although the H_2 quasi-molecular opacities were not included in these exploratory calculations. Similarly, the models used by Daou et al. (1990) did not include these opacities, an additional incentive to redo the spectroscopic analysis.

Model atmospheres and synthetic spectra were calculated in the range $T_{\rm eff}$ = 8000–17,000 K by steps of 500 K, and log g = 7.5–8.5 by steps of 0.25. Additional models at log g = 9.0 were calculated to fit LTT 4816. A pure hydrogen composition was assumed throughout. The convective efficiency was varied within the MLT, as discussed above. Even though only the ML1, ML2, and ML3 models are studied in the optical analysis, a more refined parameterization is required for the UV analysis. In this case, we adopt the constants a, b, and c from ML2 (Böhm & Cassinelli 1971), but vary α continuously. Following the nomenclature of Koester et al. (1994), we denote these models ML2/$\alpha = \alpha_0$, where α_0 is the assumed value of α (e.g., ML3 corresponds to ML2/α = 2.0; in the following ML2 $\equiv$ ML2/α = 1.0, etc.). ML1/α = 2.0 models were also computed for the comparison with the results of Koester et al. (1994; see § 3.1).

Our fitting technique is similar to that described in BSL. The first step is to normalize the line flux, in both observed and model spectra, to a continuum set to unity at a fixed distance from the line center. These normal points are chosen far enough from the line center to encompass the entire line profiles, particularly broad in ZZ Ceti stars. In BSL, the normal points were set by simply taking an average of the monochromatic flux over a few pixels. Here, we use a technique in which the spectrum is first fitted with several pseudo-Gaussian profiles (see also Saffer, Liebert, & Olszewski 1988). The normal points are then fixed at the points defined by this smooth function. This method has proven to be much more accurate when a glitch is present in the spectrum at the location where the continuum is set. It also provides a precise value of the line center which can be corrected to the laboratory wavelength. All lines from Hβ to H10 are normalized in this manner. The comparison with model spectra, which are convolved with a Gaussian instrumental profile (6 Å FWHM), is then carried out in terms of these normalized line profiles only. Here we consider only Hβ to H8 in the fitting procedure. Our minimization technique relies on the nonlinear least-squares method of Levenberg-Marquardt (Press et al. 1986), which is based on a steepest descent method.

Because of the very high S/N of our optical spectra, the internal errors of the fitting procedure are as small as 40–90 K in $T_{\rm eff}$ and 0.013–0.027 in log g. As discussed in BSL, these errors represent only the ability of the model spectra to match the data, but the error budget is actually dominated by uncertainties of the flux calibration. BSL estimated this "external" error from multiple measurements of 19 DA stars. They derived typical uncertainties of 350 K in $T_{\rm eff}$ and 0.05 in log g (or 0.03 $M_\odot$ in mass). Only G226-29 has been reobserved twice here, and the atmospheric parameters agree within 230 K in $T_{\rm eff}$ and 0.02 in log g. These differences are reassuringly smaller than the external errors estimated by BSL. As a conservative estimate, however, we assume the same uncertainties as those of BSL.

Our best fits with the ML2 version of the MLT are displayed in Figure 2*a* for the 18 ZZ Ceti stars in our homogeneous sample, and the corresponding atmospheric parameters are reported in Table 2 (top). Note the excellent quality of the simultaneous fits to all Balmer lines. The atmospheric parameters of the four additional ZZ Ceti stars discussed above are also given at the bottom of Table 2, and the line profile fits are displayed in Figure 2*b*; LTT 4816 exhibits the weaker and broader line profiles characteristic of massive stars. Surprisingly, fits obtained with ML1 and ML3 (not shown here) are undistinguishable for all stars from those obtained with ML2, although the derived atmospheric parameters strongly depend on the assumed convective efficiency (see below). Therefore, *it is not possible to constrain the convective efficiency from the quality of the optical fits.*

TABLE 2

ATMOSPHERIC PARAMETERS OF ZZ CETI STARS (ML2)

Name	WD	$T_{\rm eff}$ (K)	log g	$M/M_\odot$	M_V
R548	0133−116	13050	7.83	0.52	11.28
HL 76	0416+272	12390	7.78	0.49	11.29
G38-29	0417+361	11980	7.81	0.50	11.40
G191-16	0455+553	12300	7.93	0.57	11.52
GD 66	0517+307	13110	7.90	0.55	11.37
GD 99	0858+363	12930	7.94	0.58	11.45
G117-B15A	0921+354	12620	7.84	0.52	11.34
G255-2	1159+803	12290	8.05	0.64	11.68
GD 154	1307+354	11970	8.04	0.63	11.72
G238-53	1350+656	12950	7.76	0.48	11.20
GD 165	1422+095	13080	7.92	0.56	11.40
R808	1559+369	11960	7.93	0.57	11.57
G226-29	1647+591	13650	8.14	0.69	11.64
G207-9	1855+338	13010	8.21	0.74	11.82
G185-32	1935+276	13230	7.91	0.56	11.36
GD 385	1950+250	12750	7.90	0.55	11.41
PG 2303+243	2303+242	12400	7.96	0.59	11.54
G29-38	2326+049	12910	8.00	0.61	11.53
BPM 30551	0104−464	12080	8.11	0.68	11.81
BPM 31594	0341−459	12460	7.99	0.60	11.56
LTT 4816	1236−495	12670	8.66	1.01	12.63
L19-2	1425−811	13270	8.06	0.65	11.57

Also given in Table 2 are the mass and the absolute visual magnitude for each star. The latter have been calculated following the prescription of Wesemael et al. (1980). The masses derived here have been obtained from new evolutionary models of Wood (1995). These models have carbon-core compositions, helium layers of $M_{\rm He} = 10^{-2}\ M_*$, and thick hydrogen layers of $M_{\rm H} = 10^{-4}\ M_*$. In contrast, the models of Wood (1990) used by BSL had helium layers 100 times thinner, and no hydrogen layers[2]; these are practically equivalent to models with thin hydrogen layers ($M_{\rm H} = 10^{-10}\ M_*$). As discussed by BSL, the core composition (C or C/O) or the mass of the helium layer do not affect the derived masses significantly ($\Delta M \sim 0.004\ M_\odot$). However, the thickness of the hydrogen layer has an important effect on the inferred masses. Since there is now growing evidence that ZZ Ceti stars, and probably most DA stars as well, have thicker hydrogen envelopes than previously believed (see the discussion in Fontaine et al. 1994), we have preferred to use Wood's models with thick hydrogen layers. We estimated that the masses of the ZZ Ceti stars would be $\sim$0.026 $M_\odot$ smaller, on average, than those given in Table 2 were models with no hydrogen layers used instead.

2.4. *Determination of the Convective Efficiency Based on Optical Spectroscopy*

In Figure 3, we present the results of our $T_{\rm eff}$ and log g determinations with ML1, ML2, and ML3 models, and for 4

[2] The new models from Wood (1995) cover a range in mass of 0.4–1.0 $M_\odot$. For masses outside this range, we rely on the previous evolutionary models used in BSL.

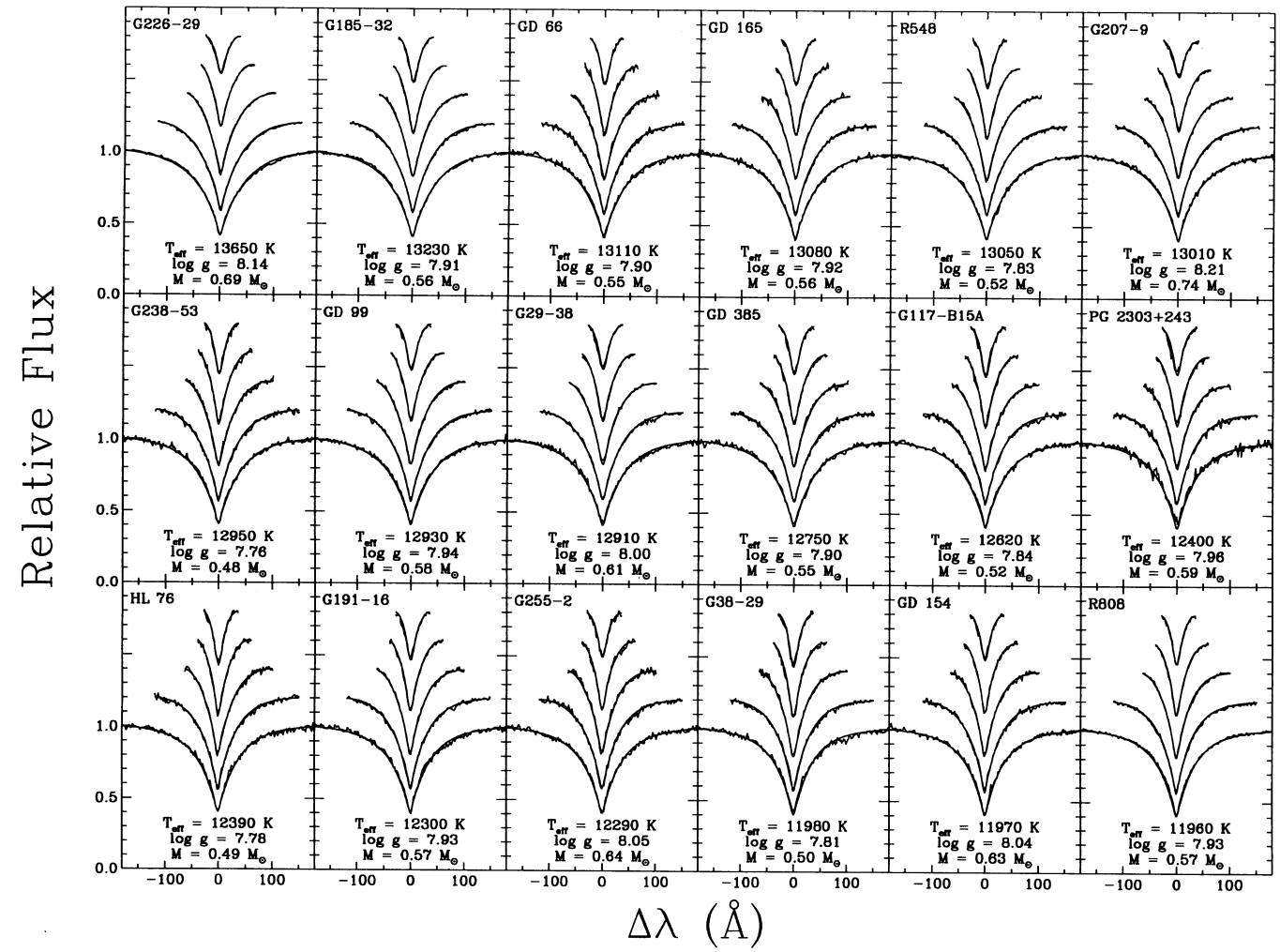

FIG. 2*a*

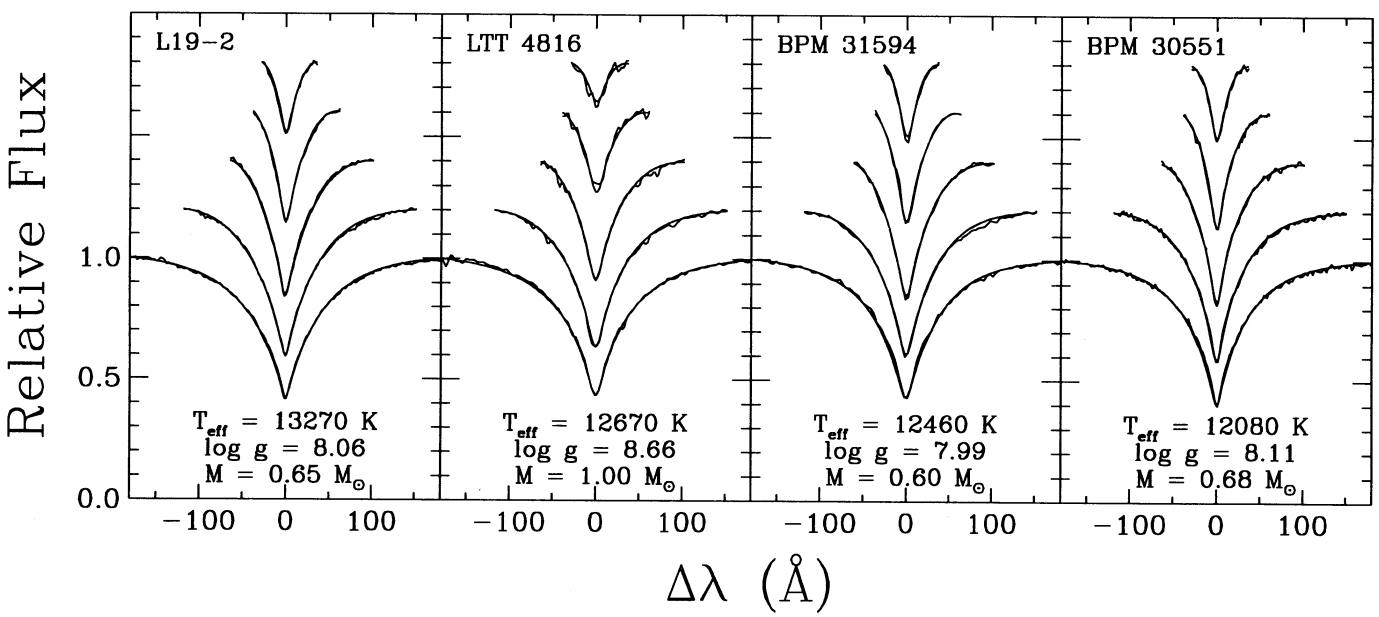

FIG. 2*b*

FIG. 2.—(*a*) Fits to the individual Balmer line profiles for our homogeneous sample of 18 ZZ Ceti stars taken from the top of Table 2. The lines range from Hβ (*bottom*) to H8 (*top*), each offset vertically by a factor of 0.2. Values of $T_{\rm eff}$ and log g have been determined from ML2 models, while the stellar masses have been derived from the models of Wood (1995) for carbon-core compositions, helium layers of $M_{\rm He} = 10^{-2}\ M_{\odot}$, and hydrogen layers of $M_{\rm H} = 10^{-4}\ M_{\odot}$. (*b*) Same as (*a*) but for the four additional ZZ Ceti stars whose optical spectra are not included in our homogeneous sample.

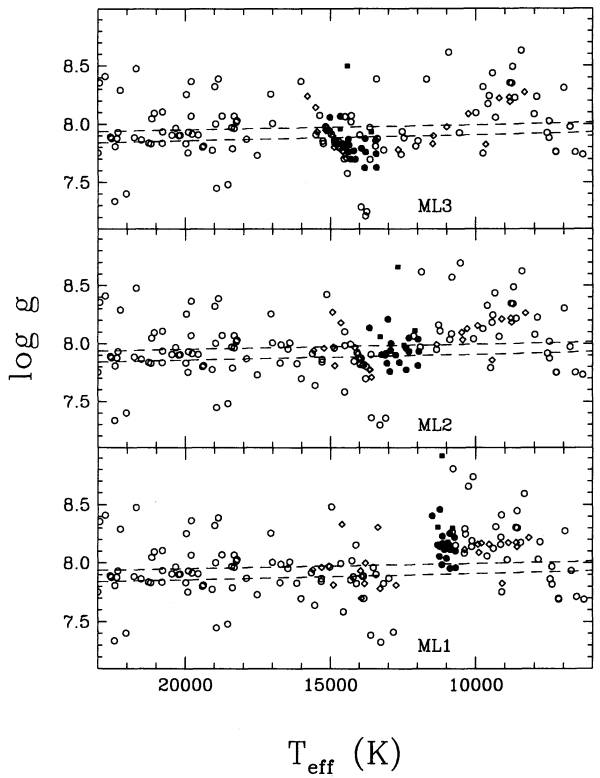

FIG. 3.—Distribution of DA white dwarfs in the $T_{\rm eff}$–log g plane for three versions of the MLT. The 22 ZZ Ceti stars from Table 1 are shown as filled symbols (*filled circles* for the first 18 ZZ Ceti stars in Table 1 and *filled squares* for the bottom four). Additional DA stars are taken from the sample of BSL (*open circles* on the hot side of the ZZ Ceti instability strip), the cool DA sample of Bergeron et al. (1990; *open circles* on the cool side of the ZZ Ceti instability strip), and the gravitational redshift sample of Bergeron et al. (1995; *open diamonds*). The dashed lines indicate the locus of the 0.55 and 0.60 $M_\odot$ evolutionary models of Wood (1995) described in the caption of Figure 2; this mass interval corresponds to the mode of the mass distribution of the 129 DA stars taken from BSL (see § 2.4).

different samples of DA white dwarfs. The first sample corresponds to the 22 ZZ Ceti stars from Table 1. The second sample is that of BSL; the coolest stars in this sample have been refitted with the same models considered here. Note that only the cool end of this sample is displayed in Figure 3, and that all objects have temperatures above the hot boundary of the ZZ Ceti instability strip. A third sample comes from the cool DA star analysis of Bergeron et al. (1990). Again, all stars have been refitted with our latest grid of model spectra; in this case, all stars fall below the red edge of the instability strip. And finally, a fourth sample comprises all the stars analyzed in the gravitational redshift study of Bergeron, Liebert, & Fulbright (1995). This sample includes all DA stars with gravitational redshift measurements, and there is thus no bias against any particular range of temperature. For instance, G117-B15A falls in this sample although we have excluded it from the gravitational redshift sample since it is already included in the ZZ Ceti sample. It is worth repeating that *all* stars below $T_{\rm eff} = 17{,}000$ K have been analyzed with a consistent set of models. In particular, the coolest stars below $T_{\rm eff} = 8000$ K have been fitted with an extension of our model grid which includes the same physics as that used for the ZZ Ceti stars, and objects around the instability strip. For the moment, we will leave aside the sample of stars cooler than the red edge of the instability strip, which will be briefly discussed in § 2.6. Several conclusions can be drawn from the results of Figure 3, and we discuss them in turn.

The atmospheric parameters of the coolest and hottest DA stars in Figure 3 do not depend on the assumed value of the MLT. As discussed by Bergeron et al. (1992b), the differences in the emergent fluxes between models calculated with different versions of the MLT are small at high effective temperatures where a negligible fraction of the energy is transported by convection, and at low effective temperatures where convection becomes adiabatic, i.e., when the thermodynamic stratification is completely specified by the adiabatic gradient. However, in the intermediate regime of temperature, and *most notably in the ZZ Ceti range*, both $T_{\rm eff}$ and log g depend strongly on the assumed parameterization of the MLT. As the convective efficiency is increased, ZZ Ceti stars become hotter and also less massive. G226-29, the hottest ZZ Ceti star in our sample, assumes values of $T_{\rm eff} = 11{,}490$, 13,650 and 15,010 K with ML1, ML2, and ML3 models, respectively. The red edge is defined by three ZZ Ceti stars with comparable effective temperatures. One of those, R808, lies at $T_{\rm eff} = 10{,}690$, 11,960, and 13,420 K with ML1, ML2, and ML3 models, respectively. Hence, from ML1 to ML3, the location of the blue edge of the ZZ Ceti instability strip increases by a full 3500 K while that of the red edge increases by $\sim$2700 K. The width of the strip with ML1 models is $\Delta(T_{\rm eff}) \sim 800$ K, a value which almost doubles with ML3 models. Also, the mean surface gravity of the 18 ZZ Ceti stars in our homogeneous spectroscopic sample decreases from a value of $\langle \log g \rangle = 8.15$ with ML1 to a value of 7.81 with ML3 models.

Another particular feature of Figure 3 is the peculiar distribution of all objects with effective temperature. In principle, the DA stars in this complete sample should be distributed more or less evenly in temperature, and form a continuous sequence as a function of $T_{\rm eff}$. However, the results of Figure 3 indicate a large gap $\sim$1500 K wide around $T_{\rm eff} = 12{,}000$ K with ML1, and a less pronounced one, $\sim$1000 K wide around $T_{\rm eff} = 16{,}500$ K with ML3. Furthermore, there appears to be a strong concentration of objects along a specific line in the $T_{\rm eff}$–log g plane around $T_{\rm eff} = 15{,}000$ K with ML3, and a less pronounced concentration with ML2 around $T_{\rm eff} = 14{,}000$ K. This last feature is not observed with ML1 models. These results can be understood qualitatively and quantitatively by looking at the variations of equivalent widths with effective temperature.

Figure 4 illustrates the variations of the equivalent width of Hγ as a function of $T_{\rm eff}$, log g, and various versions of the MLT. Also displayed is the range of equivalent widths spanned by the ZZ Ceti stars, as well as the approximate location of the maximum observed equivalent width of our complete sample of DA stars. We first note that the largest Hγ equivalent widths are not found among the ZZ Ceti population, but instead in DA stars hotter than the instability strip. A similar conclusion can be reached from the observed $[m_1, (b-y)]$ two-color diagram of Fontaine et al. (1985), reproduced here in Figure 5, where open circles represent the ZZ Ceti stars. In this plot and following figures (Figs. 6–8), we also show the results with ML2/$\alpha = 0.6$ models which are discussed later in § 3.3. The $[m_1, (b-y)]$ two-color diagram is discussed in Fontaine et al. (1985): the $(b-y)$ color index is a good temperature indicator (hotter stars are on the left side in Fig. 5), while the m_1 index measures the strength of the hydrogen Balmer lines since the Strömgren v filter in centered on the Hδ line (see Fig. 13 below,

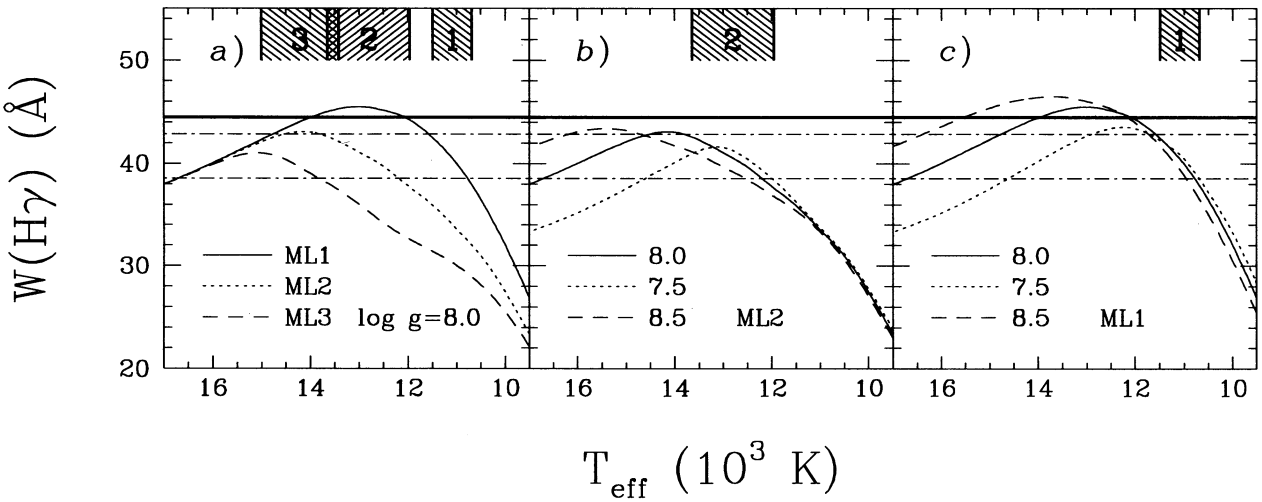

FIG. 4.—Variations of the equivalent width of Hγ with effective temperature for (*a*) log g = 8.0 models and ML1, ML2, and ML3 models; (*b*) ML2 models and log g = 7.5, 8.0, and 8.5; (*c*) same as (*b*) with ML1 models. Equivalent widths are measured with a straight line ±110 Å from the line center. The dash-dotted horizontal lines indicate the range of equivalent widths of ZZ Ceti stars, while the thick horizontal line represents the approximate maximum value of the complete sample of DA stars in Fig. 3. On top of each panel, the hatched areas indicate the range of temperatures where the ZZ Certi stars are found for a given ML*n* version.

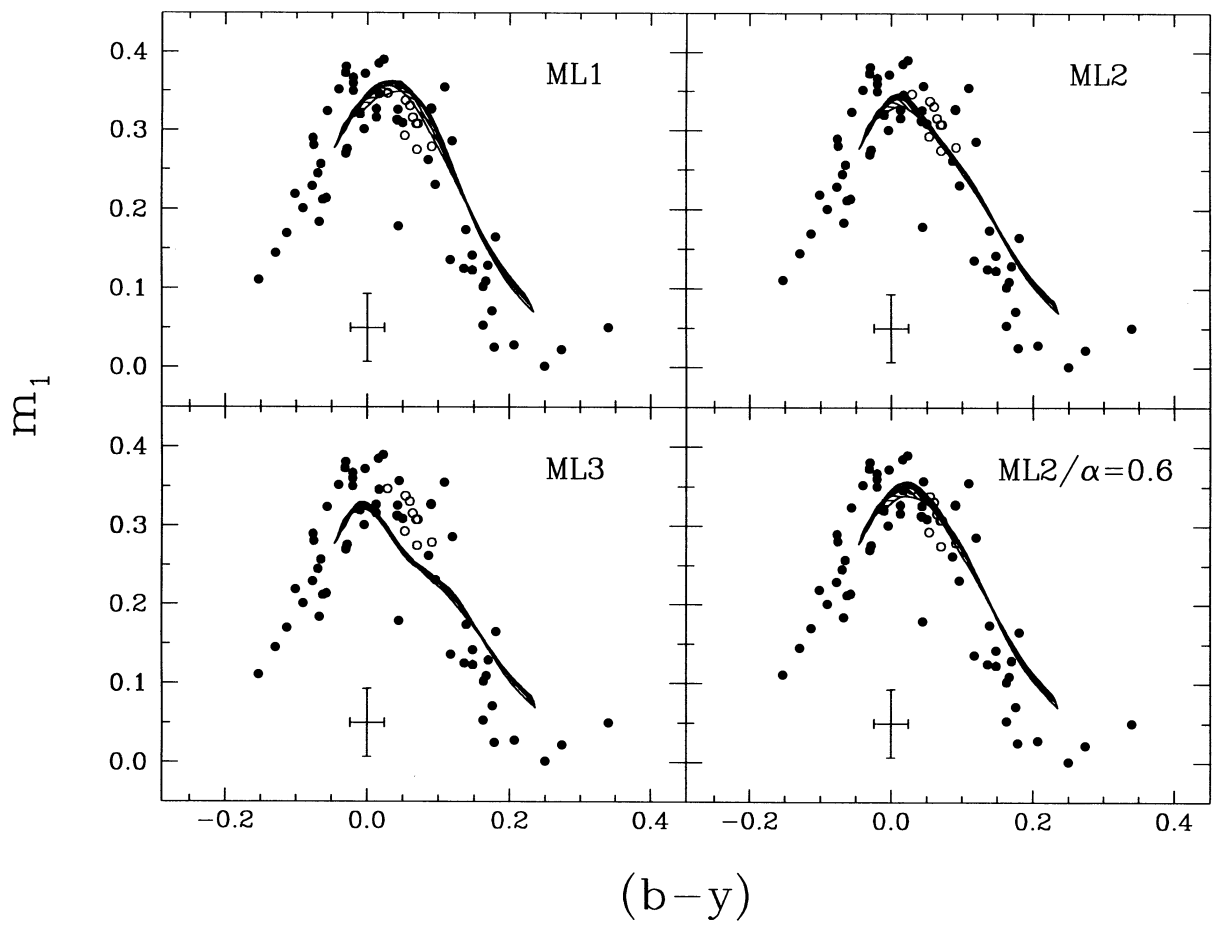

FIG. 5.—[m_1, ($b - y$)] two-color diagrams for the ML1, ML2, ML3, and ML2/α = 0.6 versions of the MLT. Models are shown for $T_{\rm eff}$ = 8000 K (*from the right*) up to 17,000 K, and log g = 7.5 to 8.5. Note that in such diagrams, the model sequences for various values of log g are superposed. The dots represent the Strömgren photometry of Fontaine et al. (1985); the open circles are ZZ Ceti stars. The cross gives the size of the error bars of the photometric measurements.

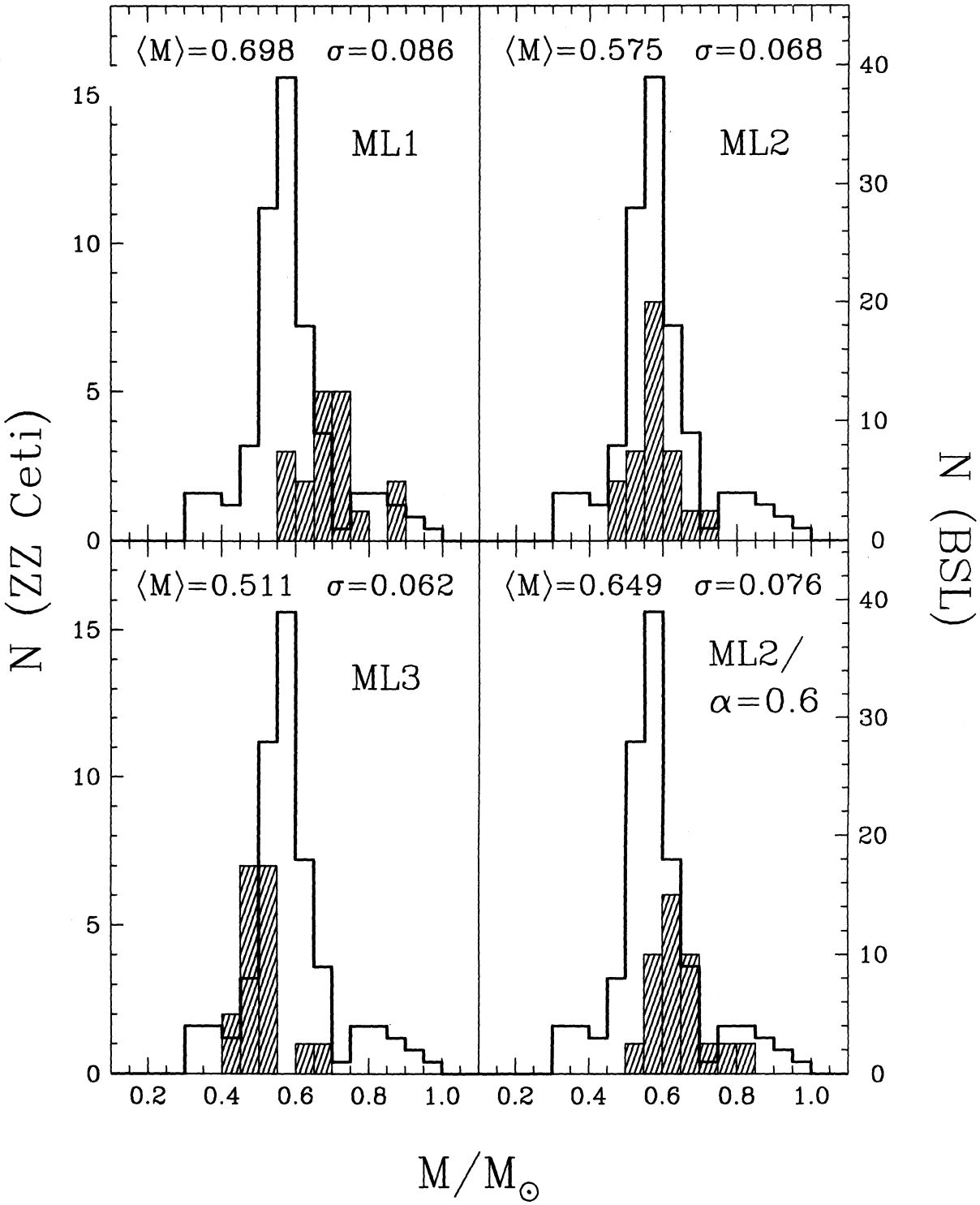

FIG. 6.—Mass distributions for our homogeneous sample of 18 ZZ Ceti stars obtained with ML1, ML2, ML3, and ML2/α = 0.6 models (*hatched histograms*). The values of the mean mass and dispersion are given in each panel in units of $M_\odot$. These mass distributions are compared with that determined here for the BSL sample of 129 warmer DA stars (*thick-line histograms*). Note the different abscissa scales for each sample. All masses have been derived from log g determinations using evolutionary models with thick hydrogen layers. The revised mean mass and dispersion for the BSL sample are $\langle M \rangle = 0.590\ M_\odot$ and $\sigma = 0.134\ M_\odot$. The ML2 parameterization yields a mean mass for the ZZ Ceti stars which best agrees with the mean value of BSL.

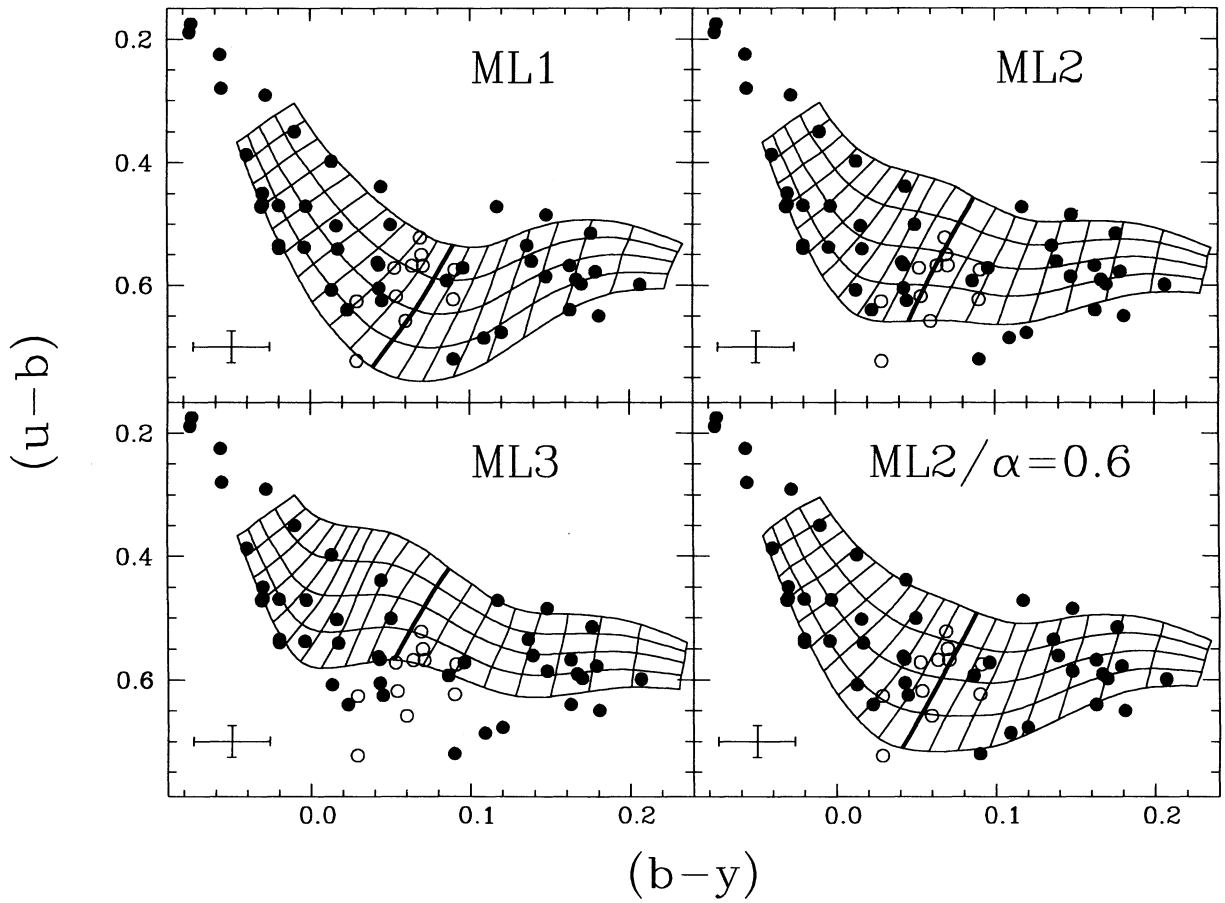

FIG. 7.—Influence of the convective efficiency on the morphology of the Strömgren [$(u - b)$, $(b - y)$] two-color diagrams. The effective temperatures range (*from right to left*) from 8000 to 17,000 K by steps of 500 K, and the values of log g (*from bottom to top*) from 7.5 to 8.5 by steps of 0.25. As a reference, the models at 12,000 K have been highlighted. The dots represent the Strömgren photometry of Fontaine et al. (1985); the open circles are ZZ Ceti stars. The cross gives the size of the error bars of the photometric measurements.

for instance). The results of Figure 5 thus indicate that the maximum in equivalent widths of the Balmer lines occur at temperatures higher than those of the ZZ Ceti stars. This important result can be used for ZZ Ceti stars to decide which of the two solutions on each side of the maximum equivalent widths is the correct one. It is *always* the coolest solution, no matter what version of the MLT is assumed.

One can see from Figure 4 that the maximum *predicted* value of the Hγ equivalent width, W_{max}, depends on both log g and the version of the MLT. The temperature at which the equivalent width reaches a maximum is also a sensitive function of these parameters. Hence, with the ML1 version of the MLT (Fig. 4*c*), W_{max} at log $g = 8.0$ is predicted larger than the maximum *observed* value for DA stars. It is therefore impossible to populate the region of the T_{eff}–log g plane where W_{max} occurs, and atmospheric parameter determinations based on ML1 models fall on each side of this maximum, thus creating a gap of objects in the temperature distribution. This is the gap observed in Figure 3, with the exception that all Balmer lines are considered there. Conversely, W_{max} in ML3 models at log $g = 8.0$ (Fig. 4*a*) is much smaller than the maximum observed value for DA stars, and even smaller than the maximum observed value for ZZ Ceti stars. Consequently, all DA stars with equivalent widths larger than W_{max}, including some of the ZZ Ceti stars, have estimated temperatures corresponding to that of W_{max}. Since the temperature at the maximum is also a function of log g (Fig. 4*b*), the stars will be concentrated on a line in the T_{eff}–log g plane, as observed with the ML2 and ML3 determinations in Figure 3. Furthermore, W_{max} with ML3 models is predicted so small that an additional gap around $T_{eff} = 16{,}500$ K is also formed where DA stars have presumably equivalent widths larger than W_{max}.

The results of Figure 4 indicate that with ML1 and ML2 models, ZZ Ceti stars are confined in a region where the equivalent widths are still growing rapidly with increasing temperature. As such, very precise T_{eff} determinations can be achieved. Moreover, since we know on which side of W_{max} lie the ZZ Ceti stars, a cool initial guess of the temperature in the fitting procedure leads to a unique and correct solution for T_{eff} and log g. Therefore, the problems encountered by Daou et al. (1990), and discussed in § 2.1, are easily avoided.

BSL have determined the mass distribution of 129 DA white dwarfs from line profile fitting techniques. With the exception of a few objects at the cool end of their sample (see our Fig. 3), most stars have atmospheres which are completely radiative, and thus their mass determinations are insensitive to the parameterization of the MLT. This is not completely true with ML3 models, however, since convection extends to much

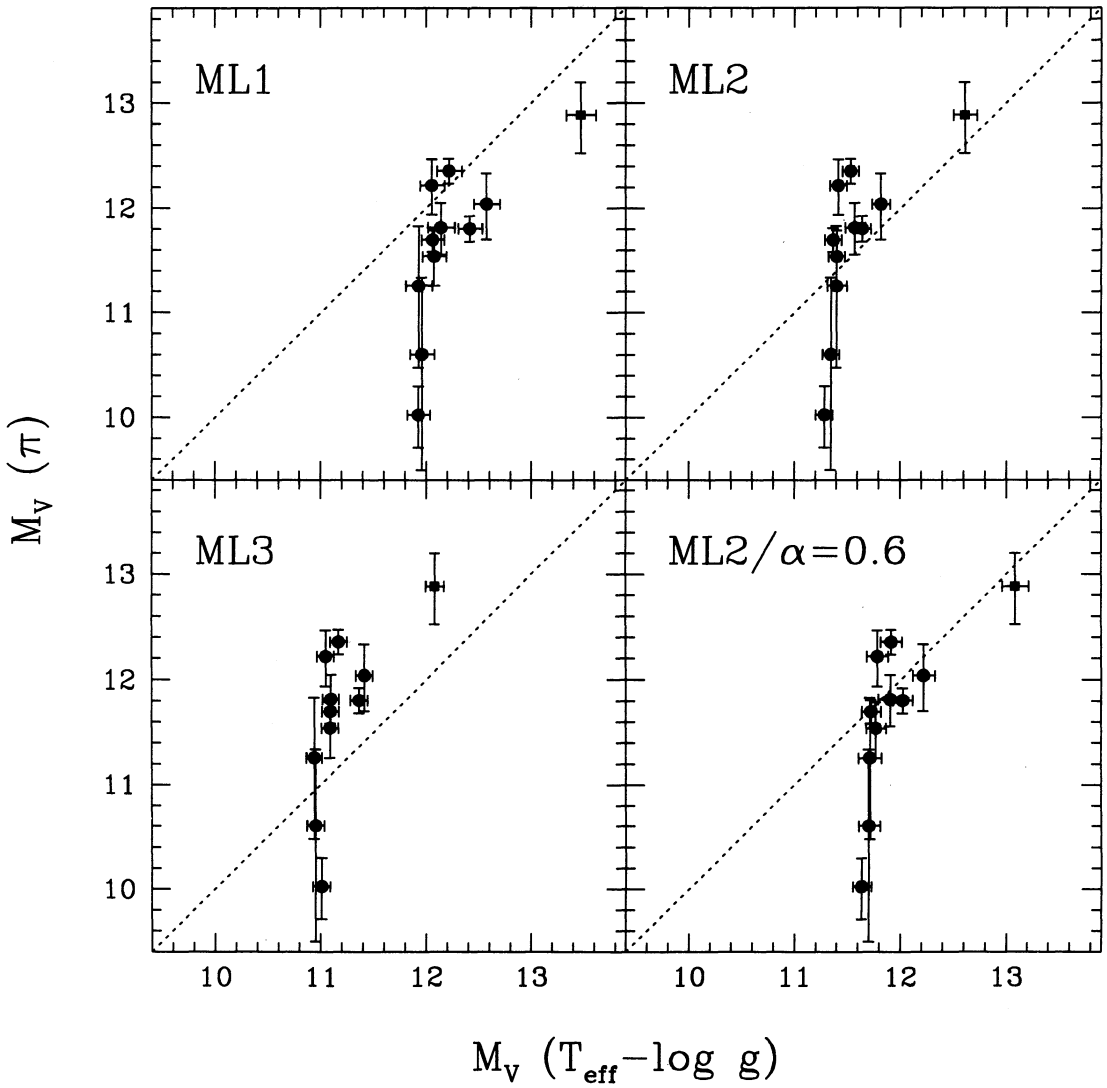

FIG. 8.—Comparison of the absolute visual magnitudes derived from trigonometric parallax measurements (Table 1) with those calculated from our $T_{\rm eff}$–log g solutions for various versions of the MLT. In each panel, the dotted line represents the 1:1 correspondence.

higher temperatures than with ML1 or ML2 models. If we assume that the mass distribution of ZZ Ceti stars is identical to that of their hotter siblings, it is possible to use the results of BSL, and in particular the value of the mean mass for DA white dwarfs, to constrain the convective efficiency in ZZ Ceti stars. In Figure 3, we show evolutionary models with a mass range corresponding to the mode of the mass distribution of DA stars (0.55–0.60 $M_\odot$; see below). It is already obvious that the ML2 parameterization provides a better match to the log g (or mass) distribution of hotter DA stars, while ML1 and ML3 models yield log g values which are respectively too large and too small.

The mass distributions can be compared more quantitatively by converting log g values into stellar masses using the models of Wood (1995) described above. We first need to recalculate the individual masses for the BSL sample, since the published values were obtained from evolutionary models with no hydrogen layer, while here we prefer to rely on models with thick hydrogen layers. The comparison of the mass distributions is displayed in Figure 6. The mass distribution of the BSL sample with thick hydrogen models has the same dispersion as that determined from thin hydrogen models [$\sigma(M) = 0.137$ $M_\odot$], but the mean value has increased from 0.562 to 0.590 $M_\odot$, and the mode of the distribution has shifted from the 0.50–0.55 $M_\odot$ mass range to 0.55–0.60 $M_\odot$. Also, more than two-thirds of the sample is now contained in a narrow mass interval of ± 0.08 $M_\odot$.

From the results of Figure 6, we conclude that the ML2 version of the MLT yields a mean mass for the ZZ Ceti stars which agrees very well with that of BSL. Note that only those 18 ZZ Ceti stars in our homogeneous spectroscopic sample are taken into account in the calculation of the mass distribution. A more refined analysis actually reveals that ML2/$\alpha = 0.9$ models yield a mean mass of 0.591 $M_\odot$ for the ZZ Ceti stars, a value identical to that of BSL. In contrast, the mean mass obtained with ML1 models (0.698 $M_\odot$) is much larger than the BSL value, while that with ML3 models (0.511 $M_\odot$) is smaller. Unless the mass distribution of ZZ Ceti stars differs significantly from that of hotter DA stars, we can conclusively exclude both the ML1 and ML3 versions of the MLT.

BSL have identified low- and high-mass tails in the mass distribution of DA stars. They have estimated that 10% of the DA white dwarfs have masses low enough ($M \lesssim 0.45\ M_\odot$) that their existence must be ascribed to close binary evolution. Some of these stars have inferred masses as low as $\sim 0.3\ M_\odot$! This low-mass tail appears to be absent in the mass distribution of the ZZ Ceti stars, although our sample is considerably smaller than that of BSL. We should nevertheless expect one or two low-mass ZZ Ceti stars, yet, none have been identified. This is a puzzling result since selection effects work in favor of discovering low-mass (larger radius) white dwarfs. The least massive ZZ Ceti star in our sample is G238-53, with a mass of $0.48\ M_\odot$ according to Table 2. On the other hand, there is at least one massive ZZ Ceti star, LTT 4816, with $M \sim 1.0\ M_\odot$ (not included in Fig. 6). This star is $\sim 0.3\ M_\odot$ more massive than the second most massive ZZ Ceti star, G207-9 ($M = 0.74\ M_\odot$). Because of the absence of the low-mass tail, and to a lesser extent of the high-mass tail, the mass dispersion of the ZZ Ceti stars is significantly smaller than that of the BSL sample.

2.5. *Internal Consistency of the ML2 Version of the Mixing-Length Theory*

Before considering the UV energy distributions of the ZZ Ceti stars, we examine additional observational constraints. Bergeron et al. (1992b) have noted previously the sensitivity of the Strömgren two-color diagrams to the assumed parameterization of the MLT. Our $[(u-b), (b-y)]$ two-color diagrams are displayed in Figure 7 for various convective efficiencies. The synthetic colors have been calculated with the sensitivity functions of Olson (1974) and the calibration of Schulz (1978). Not surprisingly, most of the effects observed in Figure 3 are reproduced here as well. Most noteworthy are the $T_{\rm eff}$ variations of the location of the ZZ Ceti instability strip, and the differences in the inferred log g values for DA stars around $T_{\rm eff} \sim 12{,}000$ K.

Perhaps of greater interest are the $[m_1, (b-y)]$ diagrams, illustrated in Figure 5 and discussed briefly in § 2.4. One of the interesting features of this two-color diagram is that the effects of log g on the predicted color indices are almost completely compensated by the effects of $T_{\rm eff}$. Hence, models with different values of log g overlap on the same sequence. This result is also consistent with the observations, within the uncertainties. We note here that the photometry of the ZZ Ceti stars of Fontaine et al. (1985) is more accurate than that of the nonvariable stars in Figures 5 and 7, since in order to obtain meaningful time-averaged colors for the variable stars, integration times were set from half an hour to more than an hour to cover a few pulsation cycles. Therefore, the size of the uncertainties for the sample of ZZ Ceti stars is actually much smaller than that indicated in Figures 5 and 7. The photometry of these 11 ZZ Ceti stars form indeed a less scattered sequence in the $[m_1, (b-y)]$ diagram than that of the nonvariable stars. The results of Figure 5 indicate that, again, ML2 provides a better description of the observations, especially in the region of the ZZ Ceti stars, while the predicted color indices for the ML1 and ML3 models pass, respectively, above and below the observed sequence.

Trigonometric parallax measurements also provide a good observational constraint against which the derived atmospheric parameters can be tested. The π values listed in Table 1 are from the new Yale parallax catalog (van Altena, Lee, & Hoffleit 1994), except that of GD 165 which is taken from Zuckerman & Becklin (1992) based on a private communication by Dahn & Harrington (1991). The results of our computation are shown in Figure 8 where we compare the absolute visual magnitudes derived directly from the trigonometric parallaxes with those inferred from our atmospheric parameter determinations. Again, the agreement with ML2 is better than with ML3, but it is somewhat comparable to that with ML1, even though the error bars are large in several instances. The largest discrepancy is for R548 (ZZ Ceti itself) for which the difference between the observed and predicted M_V values is more than 1 mag. Since R548 is neither particularly hotter or less massive (and thus brighter) than the other ZZ Ceti stars, it seems likely that the trigonometric parallax measurement for this object is in error. Alternatively, R548 could be an unresolved binary.

Spectroscopic masses can also be compared with those derived from gravitational redshift measurements. Only one ZZ Ceti star, G117-B15A, is part of a known common proper motion pair so that its redshift velocity can be measured. Bergeron et al. (1995) have compared spectroscopic and gravitational redshift masses for 35 DA white dwarfs. For G117-B15A, they find that ML2 yields a spectroscopic mass in good agreement with that inferred from the redshift velocity measured by Wegner & Reid (1991; $v_{\rm GR} = 29 \pm 6$ km s^{-1}). Since our optical spectrum and atmospheric parameter solution are somewhat different from those of Bergeron et al., we repeat the entire comparison here. Furthermore, Bergeron et al. used the evolutionary models of Wood (1990) with no hydrogen layer, while in the following we use the models of Wood (1995) with thick hydrogen layers, described in § 2.3. The inferred gravitational redshift mass is $0.596 \pm 0.074\ M_\odot$, where the uncertainty reflects the error of the redshift velocity only; the dependence on the version of the MLT is very small ($\pm 0.002\ M_\odot$). For ML1, ML2, and ML3, we obtain spectroscopic masses of 0.629, 0.519, and $0.458 \pm 0.03\ M_\odot$, respectively. Therefore, both ML1 and ML2 are within 1 σ difference (0.44 and 0.98 σ, respectively) while the ML3 value differs by $\sim 1.8\ \sigma$.

2.6. *Cool DA Stars*

A few comments on the cool DA stars below $T_{\rm eff} \sim 11{,}000$ K seem appropriate at this point. Further details will be given elsewhere. The results of Figure 3 indicate that cool DA stars appear to have larger surface gravities than their hotter counterparts. Bergeron et al. (1990) have interpreted this result as evidence for the presence of helium in the photosphere of these DA stars, brought up to the surface by convective mixing of the thin hydrogen atmosphere with the deeper and more massive helium envelope. Indeed, Bergeron et al. (1991) have shown that it is not possible spectroscopically to separate the pressure effects on the hydrogen lines originating from an increased helium abundance, from those stemming from an increased surface gravity. Helium remains otherwise spectroscopically invisible at these cool temperatures. In this context, the cool DA white dwarfs with high inferred values of log g can be alternatively interpreted as helium-enriched DA stars with normal masses. The conclusions of Bergeron et al. (1990, 1991) have been challenged occasionally since then, and we discuss some of these objections in turn.

At low temperatures, the occupation probability which governs the atomic level population is dominated by the interaction between neutral particles. In the Hummer-Mihalas formalism, this interaction is treated within a hard sphere model.

Bergeron et al. (1991) have found that this interaction was too strong, and that a line profile analysis of all the coolest DA stars required extremely low surface gravities ($\log g \ll 7.5$) as a result of the strong depopulation of the upper atomic levels. Instead, Bergeron et al. softened this interaction by reducing artificially the atomic radii of hydrogen by a factor of 2.[3]

Koester (1991) suggested that the most plausible explanation for the high log g results of Bergeron et al. (1990) was specifically this treatment of the perturbation by neutral particles. However, the contribution from the neutral particles become important *only in the coolest models*. Figure 7 of Bergeron et al. (1991) indicates that at $T_{\rm eff} = 9000$ K, the contribution of the neutral particles to the occupation probability is totally negligible in pure hydrogen models. Only below 8000 K do the neutral particle interactions become important. The results of Figure 3 show that the log g values are above average especially for DA stars hotter than 8000 K. Therefore it is implausible that the treatment of the perturbations by neutral particles in the Hummer-Mihalas formalism is at the source of the inferred high log g values.

Hammond et al. (1991) have shown that nonresonant line broadening (van der Waals interactions by neutral hydrogen) had been incorrectly neglected in our earlier calculations of the hydrogen Balmer line profiles (Bergeron et al. 1991). In the present calculations, however, we include this broadening mechanism in a manner similar to that described by Hammond et al., and our earlier conclusions about the high log g values of cool DA stars remain unchanged, as discussed above. While nonresonant broadening becomes increasingly important for higher Balmer lines, we find that Stark broadening remains always the dominant process until $T_{\rm eff}$ reaches $\sim$9000 K for Hα, $\sim$7500 K for Hβ, and $\sim$6500 K for higher Balmer lines. For $T_{\rm eff} \lesssim 6500$ K, however, the strengths of the high Balmer lines are already considerably weakened as a result of the depopulation of the higher levels by the Boltzmann factor.

Finally, the results of Figure 3 demonstrate that high log g values are inferred for the cool DA stars, regardless of the assumed convective efficiency. We can thus rule out, at this stage, any physical inaccuracies in the model calculations, and reaffirm the earlier conclusions of Bergeron et al. (1990) that the presence of helium in the atmosphere of cool DA stars is the most likely explanation for their apparent larger masses.

3. ULTRAVIOLET ANALYSIS

3.1. *Theoretical Considerations*

The UV fluxes of models near the ZZ Ceti instability strip have been illustrated, for instance, in Allard & Koester (1992). Selected results from our own calculations are displayed in Figure 9 for various values of $T_{\rm eff}$ and log g, and for various parameterizations of the MLT. These results indicate that variations of these parameters produce changes in the emergent fluxes which are qualitatively comparable. In particular, steeper energy distributions are predicted when the effective temperature is increased *or* when the surface gravity is decreased. It is therefore incorrect to conclude that a ZZ Ceti star is hot on the basis of its steep energy distribution. For instance, in Figure 1 of Wesemael et al. (1986), the UV spectrum of G226-29 appears flatter than that of G117-B15A. However, G226-29 has a higher surface gravity (log $g = 8.14$ according to Table 2) than G117-B15A (log $g = 7.84$), and as we will see below, the latter is actually the cooler of the two stars.

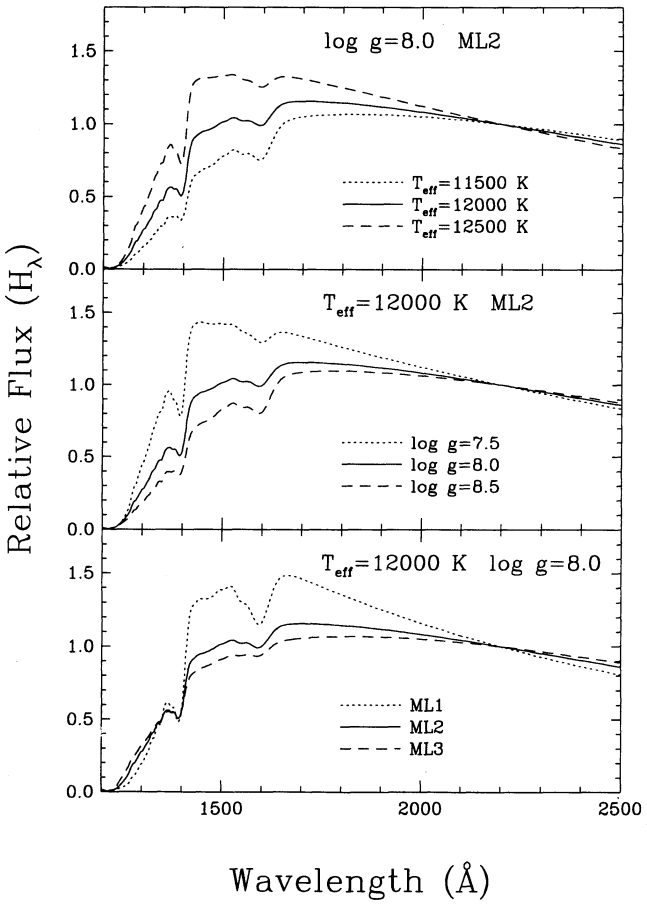

FIG. 9.—Ultraviolet energy distributions of models with various values of $T_{\rm eff}$, log g, and versions of the MLT, as indicated in each panel. All fluxes are normalized to unity at 2200 Å.

In the following, we use UV energy distributions of ZZ Ceti stars observed with *IUE* or *HST*. There are three free parameters in the fitting procedure: the effective temperature the surface gravity, and a scaling factor (R^2/D^2), which is just the square of the ratio of the radius of the star to its distance from Earth. The effects of $T_{\rm eff}$ and log g on the UV spectra can be studied more quantitatively by using observed energy distributions. In Figure 10*a*, we show our best fits to the *HST* spectrum of G117-B15A with ML2/$\alpha = 0.7$ models, and for imposed values of log $g = 7.5$ and 8.5. Surprisingly, these results demonstrate that the fits with various values of log g are virtually identical when the temperature is allowed to vary. In this case, an increase of 1 dex in log g is almost exactly compensated by increasing the value of $T_{\rm eff}$ by $\sim$1000 K. Hence, it is extremely hazardous to assign effective temperatures to white dwarf stars by assuming an average value of log g for all objects (see, e.g., Wesemael et al. 1986; Kepler & Nelan 1993). We thus conclude that it is impossible to determine a unique solution for $T_{\rm eff}$ and log g based solely on fits to the UV spectra, and one of these parameters needs to be constrained independently.

On the other hand, the variation of the predicted UV spectra with the assumed convective efficiency has a distinctive signa-

[3] We take exception, here, to the Hammond et al. (1991) description of this reduction as "reducing the quenching efficiency nearly to zero."

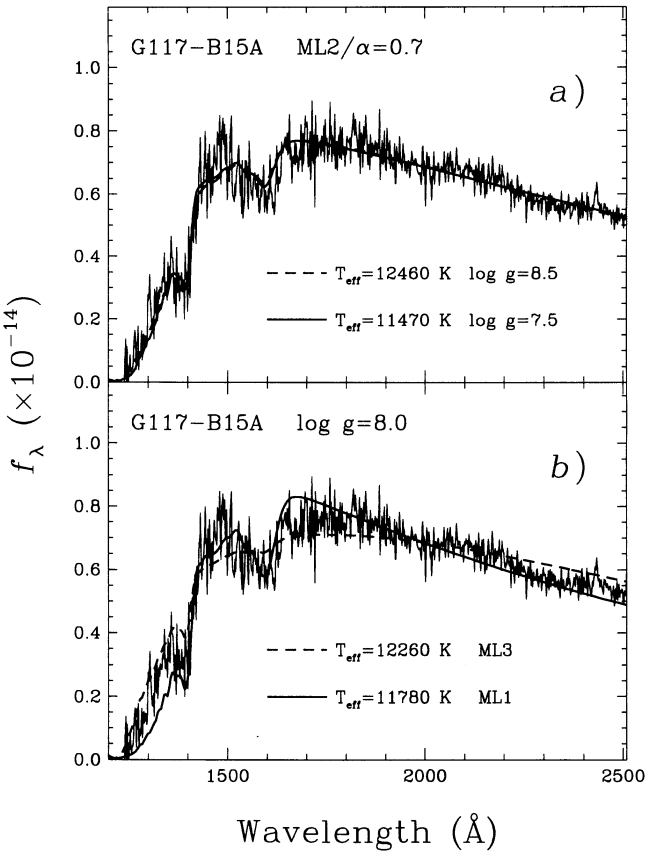

FIG. 10.—Our best fits to the UV spectrum of G117-B15A from *HST* (*a*) with ML2/α = 0.7 models and assumed values of log g = 7.5 and 8.5, and (*b*) with ML1 and ML3 models and an assumed value of log g = 8.0; only the effective temperature and the solid angle are being fitted here. Fluxes are in units of ergs cm^{-2} s^{-1} Å^{-1}.

ture. In Figure 10*b*, we show our best fits to the UV spectrum of G117-B15A with ML1 and ML3 models, and for log g = 8.0. Both fits look markedly different. The ML1 fit is steeper than the observed energy distribution in the region longward of ~1700 Å, while the flux near the center of Lyα is predicted too small. With the ML3 models, the effects are in the opposite directions. The fits to the 1400 and 1600 Å features are especially sensitive to the assumed parameterization of the MLT. Note, in particular, the weakness of the predicted 1600 Å feature with the ML3 models. These results thus demonstrate that the convective efficiency in ZZ stars can be inferred directly from the UV spectra, in contrast with the fits to the optical spectra which looked identical for various versions of the MLT. For reasons already discussed above, the quality of the fits to the UV spectra displayed in Figure 10*b* cannot be improved by assuming other values of log g.

The sensitivity of the UV fluxes to the assumed convective efficiency has been discussed in detail by Bergeron et al. (1992b): since there is less energy transported by convection in the ML1 models than in the ML3 models, the temperature gradient needs to be steeper in the former models than in the latter. The radiation flux will preferentially escape through the optically thin regions, which, in the ZZ Ceti temperature range, lie in the 1300–2000 Å region. As a result, the emergent flux of the ML1 models is larger than that of the ML3 models in the far-UV (see Fig. 9 and also Fig. 1 of Bergeron et al. 1992b).

Finally, we note that our model grid is entirely consistent with that of Koester et al. (1994), who obtain for G117-B15A, $T_{\rm eff}$ = 11,577 K, log g = 7.79, and $T_{\rm eff}$ = 12,200 K, log g = 8.12 with models calculated with ML1/α = 1.0 and α = 2.0, respectively. Assuming their derived values of log g and parameterization of the MLT, we obtain $T_{\rm eff}$ = 11,560 K and $T_{\rm eff}$ = 12,110 K, respectively, in excellent agreement with their determinations. They also obtain $T_{\rm eff}$ = 11,580 K and log g = 7.69 for G226-29 (ML1/α = 1.0), while we derive $T_{\rm eff}$ = 11,510 K under similar assumptions.

3.2. *Results with* log g *Constrained from Optical Determinations*

As mentioned above, it is not possible to determine a unique solution for $T_{\rm eff}$ and log g from fits to the UV spectra. Here we use the optical determinations from § 2.3 to constrain the surface gravity. We first assume a given version of the MLT and adopt the corresponding log g value determined from the optical spectrum. We then determine the effective temperature by fitting the UV spectrum at that value of log g. An internal consistency is reached when the optical and UV temperatures agree for a given version of the MLT.

We have performed this exercise for all ZZ Ceti stars with archival UV spectra available and for various convective efficiencies. Because the quality of these UV spectra vary widely, we assign different weights to each observation. The best exposed images are those of G117-B15A with *HST*, and those of G226-29, G185-32, and G29-38 with *IUE*. These will be assigned the highest weight. The second group with an intermediate weight is composed of G29-38 with *HST*, and G207-9, GD 99, and R808 with *IUE*. Finally, the last group with the lowest weight is composed of R548, GD 154, and GD 66 observed with *IUE*. We also assign a low weight to the *IUE* images of LTT 4816 and L19-2 since the log g determinations have been derived from the optical spectra which are not included in our homogeneous spectroscopic sample (bottom of Table 1). We do not consider the *IUE* image of G117-B15A. We thus have a total of 13 independent UV spectra. Our reduction procedure of the *IUE* images is described at length in Bergeron et al. (1994).

The comparison of UV temperatures with those derived from the optical spectra is displayed in Figure 11 for various versions of the MLT. Once the log g has been fixed at the optical value, the effective temperature obtained from the UV spectrum does not vary strongly with the convective efficiency, in contrast to the optical temperatures which vary over several thousand degrees. With the high convective efficiency of the ML3 models, the optical temperatures are ~2500 K larger than the UV temperatures. With ML2, the optical temperatures are still larger than the UV determinations, but by a lesser amount (~1000 K), while with ML1, they now become ~700 K smaller.

We find that it is possible to adjust individually the value of α for each star until the UV temperature matches the optical value. Values of α in the narrow range 0.5–0.8 embrace all the ZZ Ceti stars studied here. However, the results of Figure 11 also indicate that with ML2/α = 0.6 models, optical and UV temperatures agree within the uncertainties of the optical determinations [$\sigma(T_{\rm eff})$ ~ 350 K]. The UV and optical temperatures are compared in Table 3 for the ML2/α = 0.6 models. The agreement is even more significant if allowance is made for uncertainties of UV temperature determinations as well. Therefore, we conclude that it is possible to achieve an internal consistency between optical and UV temperatures

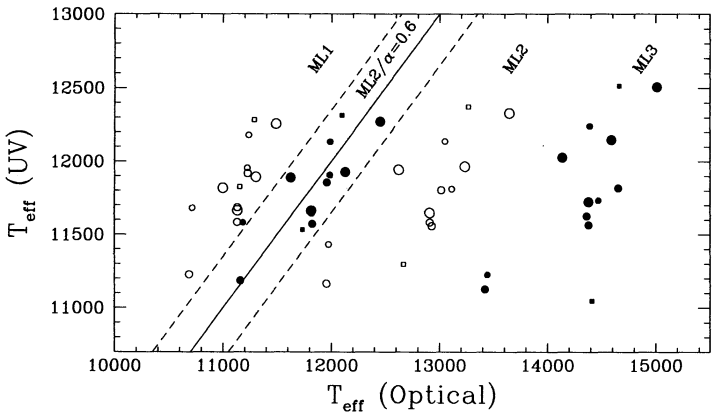

FIG. 11.—Effective temperatures derived from UV spectra compared with the optical determinations. Results are displayed for various parameterizations of the MLT; for clarity, the results are shown with alternate open/filled symbols. Optical log g values are assumed in the determination of the UV temperatures. The size of the symbols reflects the different weights assigned to the UV spectra, as discussed in the text. The squares represent LTT 4816 and L19-2 whose optical spectra are not included in our homogeneous spectroscopic sample. The solid line indicates the locus where T_{eff}(optical) = T_{eff}(UV), while the dashed lines represent the ±350 K uncertainty allowed by the optical analysis.

within the MLT by using models parameterized with ML2/α = 0.6. It is worth mentioning that this internal consistency does not necessarily guarantee a good fit to the UV spectra.

Fortunately, ML2/α = 0.6 models do provide excellent fits to the UV spectra as shown in Figure 12 for the four best exposed images. These fits could be improved marginally by fine tuning the value of α for each star, and especially in the region around the 1400 Å feature, but considering the overall uncertainties of our analysis, the quality of these fits is more than satisfactory. Fits to the other ZZ Ceti stars (not displayed here) are in good agreement with the observations as well.

3.3. *Internal Consistency of the* ML2/α = 0.6 *Version of the Mixing-Length Theory*

As we have seen in the previous sections, the ML2/α = 0.6 models provide good fits to the UV and optical spectra, and yield UV temperatures which are consistent with the optical determinations. Since UV spectra are not available for all ZZ Ceti stars, we rely in the following exclusively on T_{eff} and log g determinations derived from optical spectroscopy. The optical determinations with the ML2/α = 0.6 models are reported in Table 4. It now remains to verify that these solutions also satisfy the additional constraints explored in § 2.5.

TABLE 3

T_{eff} DETERMINATIONS FROM UV SPECTRA (ML2/α = 0.6)

Name	Source	T_{eff} (K)	ΔT_{eff} (UV − Opt)
G117-B15A	*HST*	11890	+270
G29-38	*IUE*	11660	−160
G226-29	*IUE*	12270	−190
G185-32	*IUE*	11930	−200
G29-38	*HST*	11650	−170
G207-9	*IUE*	11860	−100
GD 99	*IUE*	11570	−250
R808	*IUE*	11180	+20
R548	*IUE*	12130	+140
GD 154	*IUE*	11580	+400
GD 66	*IUE*	11910	−70
L19-2	*IUE*	12310	+210
LTT 4816	*IUE*	11530	−200

TABLE 4

ATMOSPHERIC PARAMETERS OF ZZ CETI STARS (ML2/α = 0.6)

Name	WD	T_{eff} (K)	log g	$M/M_\odot$	M_V
R548	0133−116	11990	7.97	0.59	11.63
HL 76	0416+272	11440	7.89	0.55	11.63
G38-29	0417+361	11180	7.91	0.55	11.71
G191-16	0455+553	11420	8.05	0.64	11.86
GD 66	0517+307	11980	8.05	0.64	11.75
GD 99	0858+363	11820	8.08	0.66	11.83
G117-B15A	0921+354	11620	7.97	0.59	11.70
G255-2	1159+803	11430	8.17	0.71	12.04
GD 154	1307+354	11180	8.15	0.70	12.07
G238-53	1350+656	11890	7.91	0.55	11.56
GD 165	1422+095	11980	8.06	0.65	11.77
R808	1559+369	11160	8.04	0.63	11.91
G226-29	1647+591	12460	8.29	0.79	12.02
G207-9	1855+338	11960	8.35	0.83	12.22
G185-32	1935+276	12130	8.05	0.64	11.73
GD 385	1950+250	11710	8.04	0.63	11.78
PG 2303+243	2303+242	11480	8.09	0.66	11.90
G29-38	2326+049	11820	8.14	0.69	11.91
BPM 30551	0104−464	11270	8.22	0.74	12.16
BPM 31594	0341−459	11540	8.11	0.67	11.92
LTT 4816	1236−495	11730	8.81	1.09	13.10
L19-2	1425−811	12100	8.21	0.74	11.96

We first consider the internal consistency with the Strömgren photometry. In the [m_1, ($b - y$)] two-color diagram (Fig. 5), the ML2/α = 0.6 models reproduce very nicely the observed location of the ZZ Ceti stars, an even better match than with the ML1, ML2, or ML3 models. Moreover, the mean surface gravity of all ZZ Ceti stars in Table 4 is $\langle \log g \rangle$ = 8.12, a value which is certainly consistent with the location of the 11 observed ZZ Ceti stars in the [($u - b$), ($b - y$)] diagram (Fig. 7). In Table 4, the instability strip is defined on the cool side by R808 at T_{eff} = 11,160 K, and on the hot side by G226-29 at T_{eff} = 12,460 K. The location and the width of the ZZ Ceti instability strip is thus in good agreement with the results of Figure 7 with ML2/α = 0.6. We note, however, that in the [($u - b$), ($b - y$)] diagram, several stars fall above T_{eff} = 12,000 K, while only 3 ZZ Ceti stars are found above that temperature in Table 4. On the other hand, the mean temperatures are consistent within the uncertainties of ($b - y$).

We have also found a good agreement with the absolute photometry but only for the best exposed UV images, a result which strongly suggests that the absolute UV fluxes are not always reliable. Furthermore, as discussed by Koester et al. (1994), the small aperture and the spherical aberration of *HST* renders the absolute flux level of the FOS observations somewhat uncertain. We find that the FOS observations of G117-B15A need to be multiplied by a factor of ~1.4 for our predicted fluxes to match the observed Strömgren and Johnson V photometry. A factor of 1.63 was derived by Koester et al. from a comparison of the FOS spectrum and the average *IUE* spectrum of G117-B15A. However, the latter image is seriously underexposed. Our best examples of the internal consistency with the observed photometry are illustrated in Figure 13, where the Strömgren u, v, b, and y from Fontaine et al. (1985), as well as the Johnson V photometry from Table 1, have been converted to monochromatic fluxes using the calibration of Heber et al. (1984).

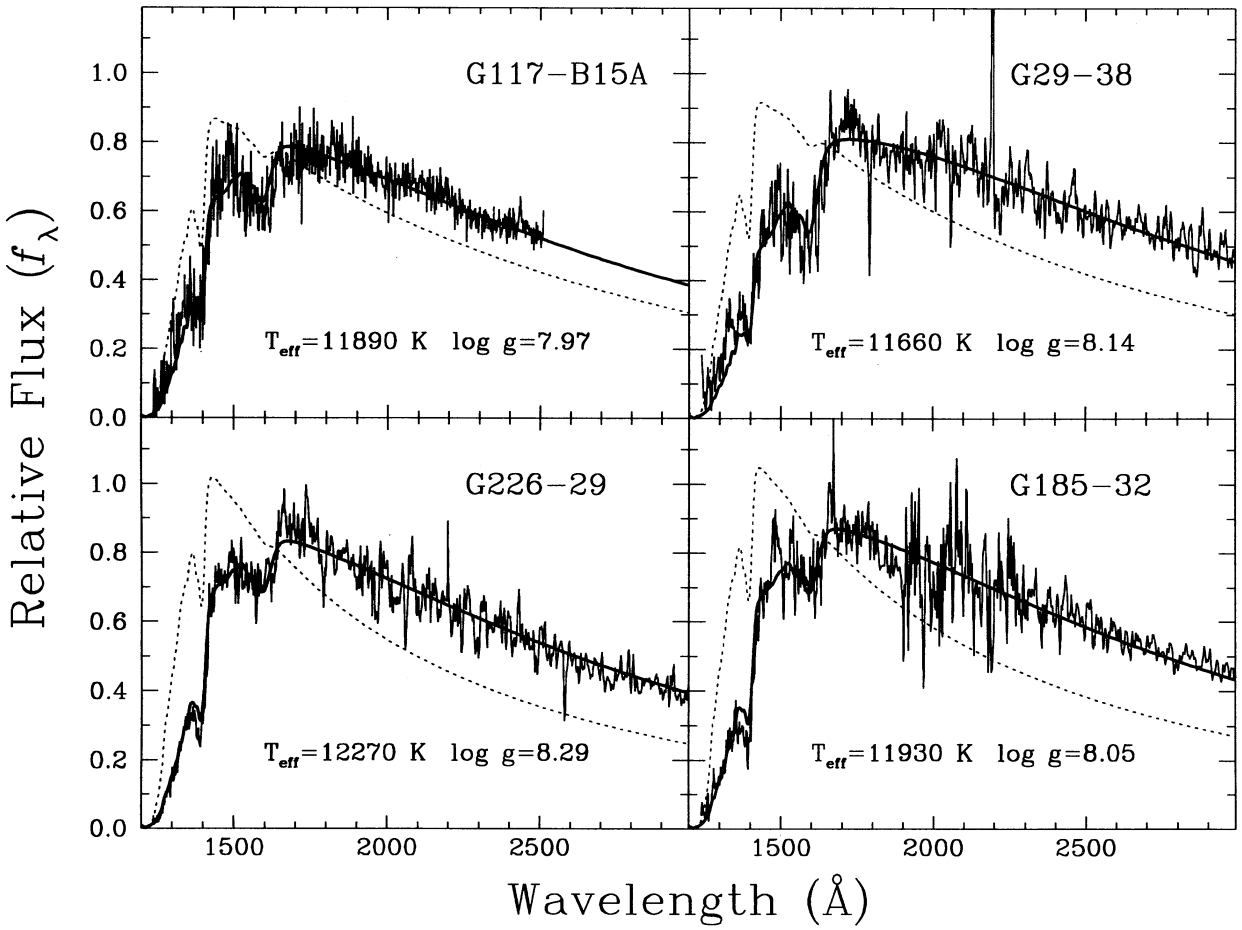

FIG. 12.—Our best fits to the four ZZ Ceti stars with the highest signal-to-noise UV spectra. The solid lines and the atmospheric parameters indicate our solutions with ML2/α = 0.6 models; $T_{\rm eff}$ and the solid angle are free parameters in the fitting procedure while log g is taken from the optical determination. The dotted lines represent our fits when both $T_{\rm eff}$ and log g are taken from the ML2 optical determinations; only the solid angle is being fit here.

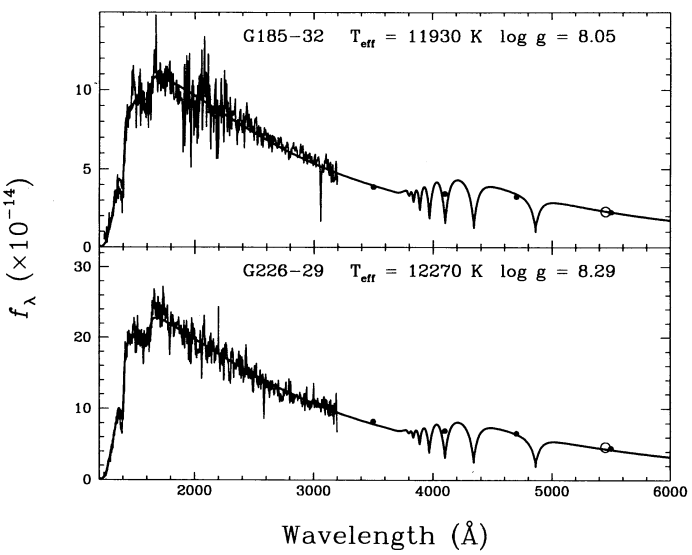

FIG. 13.—Our best fits to the UV spectra of G185-32 and G226-29 with ML2/α = 0.6 models. Fluxes are in units of ergs cm^{-2} s^{-1} Å^{-1}. The dots and the open circle represent the Strömgren *uvby* and Johnson *V* photometry, respectively. The photometry is shown here as a comparison but it is not used in the fitting procedure.

The results of Figure 8 also indicate that ML2/α = 0.6 models yield absolute visual magnitudes which agree, on average, with the values obtained from trigonometric parallax measurements. And finally, we have already discussed the comparison between the spectroscopic mass of G117-B15A and that inferred from gravitational redshift measurements. Interestingly enough, the spectroscopic mass obtained with ML2/α = 0.6 models agree with the gravitational redshift mass within 0.06 σ! Therefore, we conclude that ML2/α = 0.6 provide an overall internal consistency between optical and UV spectroscopy, color indices, absolute photometry, trigonometric parallaxes, and gravitational redshifts (at least for one star in the latter case).

The mass distribution of the ZZ Ceti stars derived with ML2/α = 0.6 models is significantly different from that of BSL, however, and thus different from that of hotter normal DA stars. Figure 6 indicates that the mean mass of the ZZ Ceti stars is $\sim$0.06 $M_\odot$ larger than that of BSL. Since there is no reason to expect the mass distribution of DA stars in the ZZ Ceti temperature range to differ from that of hotter DA stars, we are unavoidably forced to conclude, in the light of our analysis, that in order to preserve the value of the mean mass, the ZZ Ceti instability strip is necessarily contaminated with nonvariable stars with lower masses. If this interpretation is

correct, the relative mass distributions in Figure 6 suggest that only ~40% of the DA stars within the ZZ Ceti instability strip should be variable, a result which is clearly at odds with the photometric evidence of the purity of the ZZ Ceti instability strip (Fontaine et al. 1982; Greenstein 1982). We note that none of these purported lower mass, nonvariable DA stars within the ZZ Ceti instability strip have been identified in our sample, with the exception of two or three very low mass white dwarfs close to the blue edge. These issues are further discussed in § 4.1.

We found in § 2.4 that ML2 models yield a mass distribution in close agreement with that of BSL. To illustrate how impossible it is to reconcile this parameterization of the MLT with the UV analysis, we also show in Figure 12 our fits to the UV spectra by using the ML2 optical solutions for $T_{\rm eff}$ and log g, i.e., only the solid angle is adjusted here. These results clearly illustrate the inadequacy of the ML2 models to fit the UV energy distributions.

4. DISCUSSION

4.1. *ZZ Ceti Instability Strip*

Figure 9 of Tassoul et al. (1990) illustrates the convection zone profiles and thermal timescales at the base of the convection zone as a function of effective temperature for 0.6 $M_\odot$ DA sequences and various versions of the MLT. At a given temperature, the base of the convection zone is deeper for models with a larger convective efficiency, and the corresponding thermal timescales at the base of the convection zone are thus longer. The blue edge of the instability strip corresponds approximately to the effective temperature at which the base of the convection zone is sufficiently deep for the thermal timescale to be comparable with the shortest observable g-modes, typically 100 s (see, e.g., Winget & Fontaine 1982; Fontaine, Tassoul, & Wesemael 1984). For instance, the thermal timescale reaches a value of $\tau_{\rm th} = 100$ s at $T_{\rm eff} \sim 10{,}000$ K in ML1 models, while the same value is reached at $T_{\rm eff} \sim 12{,}000$ and 12,800 K in ML2 and ML3 models, respectively. Hence, the *observational* determination of the boundaries of the ZZ Ceti instability strip is of particular interest since the temperature of the blue edge, as inferred from envelope models, should help constrain the convective efficiency in the deeper layers.

Our atmospheric parameter determinations for the ZZ Ceti stars are reproduced in Figure 14*a* for the ML2 and ML2/$\alpha = 0.6$ models, together with the theoretical blue edges for various versions of the MLT. These theoretical predictions are taken from the recent stability survey of Brassard et al. (1995a), a study similar to that described in Fontaine et al. (1994), in which the system of ordinary differential equations which describes the linear, nonadiabatic, nonradial pulsations of stellar models is solved in detail through finite-element techniques. These studies have shown, in particular, that the theoretical blue edge of the ZZ Ceti instability strip does not depend on the hydrogen layer mass for $M_{\rm H} \gtrsim 10^{-12}\ M_\odot$ (see also Bradley & Winget 1994a for a similar result). Also shown in Figure 14*a* are the predictions for adiabatic models which represent the upper limit for the convective efficiency. Our $T_{\rm eff}$ determinations with ML2 or ML2/$\alpha = 0.6$ models are reassuringly below this limit.

More important, the stability results in Figure 14*a* indicate that the effective temperature at the blue edge is a sensitive function of the stellar mass (see also Bradley & Winget 1994a), and may vary by as much as ~1500 K over a range of 1 dex in log g. Therefore, the most massive ZZ Ceti stars at the blue edge of the instability strip should be hotter than the less massive stars. Interestingly enough, this is precisely what is observed, whether the ML2 or ML2/$\alpha = 0.6$ results are considered. With the ML2/$\alpha = 0.6$ models, there are four stars which are well aligned with the blue edge predicted from the ML2 *envelope* models. In order of decreasing effective temperatures and surface gravities, these are G226-29, G185-32, R548, and G238-53, while L19-2, GD 66, and GD 165 form the next group at slightly cooler temperatures. In this context, *we are forced to conclude that convection in the upper atmosphere is less efficient than in the deeper envelope*, a result consistent with the recent numerical simulations of convective energy transport at the surface of ZZ Ceti stars by Ludwig, Jordan, & Steffen (1994). These authors found from their two-dimensional hydrodynamic calculations that it was not possible to reproduce the temperature profile of a $T_{\rm eff} = 12{,}600$ K, log $g = 8.0$ atmosphere and envelope model with a single value of α. Instead, the temperature profile is better represented by models with values of α increasing toward the interior. We note that a similar conclusion can be reached from Figure 14*a* even with our ML2 results. In this case, the envelope models require a convective efficiency larger than that provided by the ML3 parameterization, and close to that of the adiabatic models.

There is still no theoretical explanation for the existence of a red edge in the ZZ Ceti instability strip. However, it has been argued that the onset of convective mixing between the relatively thin hydrogen layer and the more massive helium layer

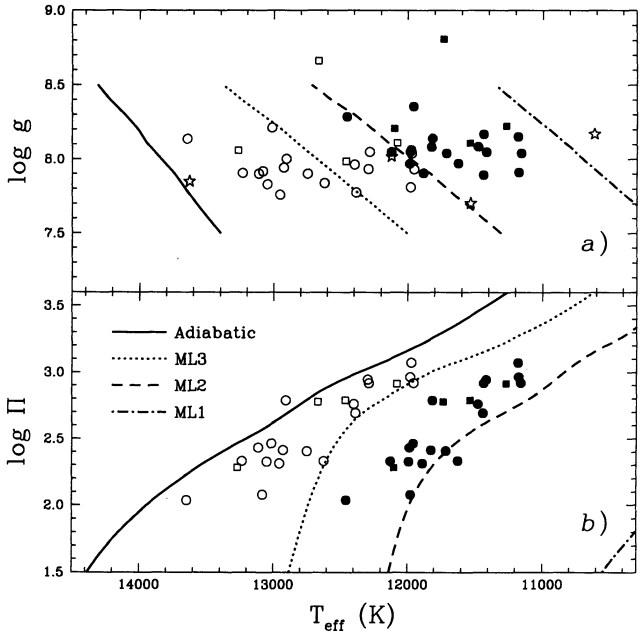

FIG. 14.—(*a*) Atmospheric parameter determinations for the 22 ZZ Ceti stars with ML2 models (*open symbols*) and ML2/$\alpha = 0.6$ models (*filled symbols*); BPM 31594; BPM 30551, L19-2, and LTT 4816 are indicated by squares. The star symbols represent the four nonvariable DA stars from Kepler & Nelan (1993) discussed in § 4.1; these are fitted with the ML2/$\alpha = 0.6$ models only. The theorerical blue edges obtained from the nonadiabatic calculations of Brassard et al. (1995) are indicated for ML1, ML2, and ML3 models, as well as for adiabatic stratifications. (*b*) Distribution of the ZZ Ceti stars in the $T_{\rm eff}$–period diagram for the ML2 and ML2/$\alpha = 0.6$ determinations. The periods (Π) are in seconds and represent the value of the dominant pulsation mode listed in Table 1. Here, the curves indicate the thermal timescales at the bottom of the convection zone of the 0.6 $M_\odot$ models of Tassoul et al. (1990).

around $T_{\rm eff} \sim 11{,}000$–$12{,}000$ K could turn a DA star into a non-DA star or a helium-rich DA star (Winget & Fontaine 1982; Bergeron et al. 1990), and could thus account for the existence of a red edge. However, convective mixing at such high effective temperatures requires extremely thin hydrogen layers of $M \sim 10^{-14}$ to 10^{-11} $M_\odot$ (Fontaine & Wesemael 1991). This range of mass is significantly smaller than values inferred for at least two ZZ Ceti stars: For G226-29, Fontaine et al. (1992) inferred a hydrogen layer mass of $M({\rm H}) \sim 10^{-4.4}$ M_* for $l = 1$, while for GD 165, Bergeron et al. (1993) found $M({\rm H})/M_* \gtrsim 10^{-3.7}$ or $\gtrsim 10^{-6.4}$ if the 120 s pulsation is a mode with $l = 1$ or 2, respectively. Other explanations for the existence of the red edge invoke the interaction of pulsation with convection (e.g., Winget & Fontaine 1982).

There is thus currently no information available whether the temperature of the red edge depends on stellar mass. The results of Figure 14*a* suggest, however, that there is no strong variation of $T_{\rm eff}$ with log g at the red edge. Our red edge is located at $T_{\rm eff} = 11{,}950$ and 11,150 K for ML2 and ML2/$\alpha = 0.6$ models, respectively, and is defined by three stars, G38-29, GD 154, and R808. It is worth not mentioning at this point that the ordering of ZZ Ceti stars in terms of effective temperature or mass does not vary significantly between ML2 and ML2/$\alpha = 0.6$ models, so that the blue and red edges are defined by the same stars with both parameterizations of the MLT.

Some interesting conclusions can be drawn if we assume that the effective temperature at the red edge of the ZZ Ceti instability strip has no dependence, or a weak dependence on the stellar mass. In the following, we consider only the ML2/$\alpha = 0.6$ results from Figure 14*a*, but these conclusions can be extended to any parameterization of the MLT. We thus place the red edge at $T_{\rm eff} \sim 11{,}200$ K. First, the width of the instability strip is a function of log g, or equivalently, of the stellar mass. For instance, it is ~ 1500 K wide at log $g = 8.3$ (the log g value of G226-29), but as narrow as ~ 700 K at log $g = 7.9$ (the log g value of the lowest mass ZZ Ceti star). This strong dependence also implies that no ZZ Ceti stars should exist below log $g \sim 7.4$, the locus where the predicted ML2 blue edge intersects the observed red edge. This conclusion is consistent with our findings. Second, because of this log g dependence, the probability of finding low-mass ZZ Ceti stars is much smaller than that of finding massive ZZ Ceti stars. This result could explain, at least in part, our conclusion that the mean mass of ZZ Ceti stars with ML2/$\alpha = 0.6$ models is ~ 0.06 $M_\odot$ larger than the mean of hotter DA stars.

It is possible to explore this assertion more quantitatively by performing the following experiment. We use the mass determinations of the 129 DA stars from the BSL analysis, and distribute them randomly within the temperature interval defined by the hottest and coolest ZZ Ceti stars ($12{,}460 \leq T_{\rm eff} \leq 11{,}160$ K with ML2/$\alpha = 0.6$); we actually use cooling timescales to distribute the objects, but we find that this effect is small over the range of $T_{\rm eff}$ considered. Then we use the theoretical ML2 blue edge from Figure 14, converted into stellar mass, to exclude from our simulated $T_{\rm eff}$ and mass distributions all DA stars hotter than the theoretical blue edge. We then recalculate the mean mass for this new sample which is now biased toward higher masses. Since this is a random procedure, we repeat the simulation several times. We find that the mean mass increases from 0.590 $M_\odot$ to a "corrected" value of 0.631 $M_\odot$, in much better agreement with the value derived from the ZZ Ceti stars (0.649 $M_\odot$). In fact, a Student's t-test analysis reveals that the sample of ZZ Ceti stars has only a $\sim 7\%$ probability of having the same mean mass as the BSL sample, while this probability jumps to $\sim 60\%$ with our corrected mass distribution. Since we are still dealing with a very small number of objects to define the mass distribution of ZZ Ceti stars, we conclude that the difference in the mass distributions observed in Figure 6 is simply a selection effect resulting from the mass dependence of the theoretical blue edge of the ZZ Ceti instability strip (with a fixed red edge).

It is clear from these results that the concept of a "canonical effective temperature of the blue edge" is somewhat misleading. A simultaneous determination of $T_{\rm eff}$ and log g is required before claiming that any given star lies within the instability strip. For instance, we expect to find several DA stars slightly cooler than G226-29, the hottest ZZ Ceti star, but with surface gravities lower than the values defined by the theoretical boundary. There are at least five DA stars in Figure 3 (ML2 panel) with temperatures slightly lower than G226-29, but as expected, they have lower surface gravities as well. Three of them are extremely low-mass stars ($M \sim 0.3$ $M_\odot$). DA stars hotter than the blue edge are difficult to identify from optical spectroscopy alone, however, since these objects lie very close to the maximum of the equivalent width, and thus, the problem encountered by Daou et al. (1990), where two solutions are possible, reappears. Hence, a detailed study of stars hotter than the blue edge of the ZZ Ceti instability strip requires UV spectroscopy to better constrain the temperature determination.

Kepler & Nelan (1993) have claimed the identification of four nonvariable DA stars within the ZZ Ceti instability strip. These are BPM 2819, LP 550-52, BPM 20383, and G8-8. The spectra of the first three objects are available to us from the analysis of Bragaglia et al. (1995), while that of G8-8 has been obtained at the Steward Observatory. We have performed the same optical and UV analyses for these four objects using the ML2/$\alpha = 0.6$ models, the results of which are reported in Table 5. Except for BPM 20383 for which the UV spectrum is extremely noisy, the UV and optical temperatures agree within the optical uncertainties. The effective temperatures of LP 550-52 and BPM 20383 (LTT 4013) obtained by Bragaglia et al. (1995) are significantly hotter than those obtained here, implying that the solutions they adopted are those on the hot side of the maximum of the equivalent widths, a result which stresses the importance of combining optical and UV data for DA stars in this range of effective temperature. Our atmospheric parameter determinations for these four stars are shown in Figure 14*a* as star symbols. BPM 2819 and BPM 20383 are clearly outside the instability strip, while LP 550-52 and G8-8 are located exactly at the blue edge. Hence the atmospheric parameters of these two nonvariable DA white dwarfs do not overlap with those of the variable stars, even though they are located within the temperature interval of the ZZ Ceti stars. Therefore, such stars *do exist*. An optical and UV survey

TABLE 5

ATMOSPHERIC PARAMETERS FOR THE KEPLER-NELAN DA STARS (ML2/$\alpha = 0.6$)

WD	Name	$T_{\rm eff}$/UV (K)	$T_{\rm eff}$/Opt (K)	log g	$M/M_\odot$
0255−705.....	BPM 2819	10961	10620	8.17	0.71
0401+250.....	G8-8	12227	12120	8.02	0.62
1022+050.....	LP 550-52	11779	11540	7.70	0.45
1053−550.....	BPM 20383	12849:	13630	7.85	0.53

of DA stars close to the blue edge of the instability strip would help to determine whether there are sufficient lower mass DA stars in this region of the $T_{\rm eff}$–log g plane to restore the mass distribution of BSL in this range of effective temperatures.

4.2. *Effective Temperature–Period Relation*

As ZZ Ceti stars cool down through the instability strip, the base of the convection zone reaches deeper regions in the envelope, and the corresponding thermal timescales become longer. As such, longer period modes can be driven in cooler ZZ Ceti stars, leading to the predicted $T_{\rm eff}$–period relation. Previous observational evidence for such a correlation are suggested in Figure 4 of Winget & Fontaine (1982) and Figure 5 of Wesemael et al. (1986). The results of our analysis, displayed in Figure 14*b*, exhibit the strongest $T_{\rm eff}$–period relation ever uncovered, with all stars aligned on a tight sequence. This remarkable result strengthens our confidence in the relative temperature scale achieved with the optical spectra. Also shown are the thermal timescales taken from Figure 9 of Tassoul et al. (1990) for various versions of the MLT, and for adiabatic models as well. Since the thermal timescale gives only a rough estimate of the shortest modes that can be driven at the base of the convection zone (the exact values can be several times the thermal timescales; see, e.g., Brickhill 1991), the results of Figure 14*b* are entirely consistent with those of Figure 14a. For instance, the ML2 thermal timescales provide a good match to the $T_{\rm eff}$–period data from the ML2/α = 0.6 analysis. G226-29 with the observed shortest dominant period is also the hottest ZZ Ceti star in our sample.

4.3. *Consistency of the* ML2/α = 0.6 *Models with Hotter DA Stars*

Even though the atmospheres of DA stars hotter than the blue edge are less convective than those of ZZ Ceti stars, their atmospheric parameters are still strongly dependent on the parameterization of the MLT. For instance, a comparison of the ML1 and ML3 results in Figure 3 reveals that the atmospheric parameters of DA stars as hot $T_{\rm eff} \sim 17{,}000$ K are still model dependent. It is thus possible to verify the internal consistency of the ML2/α = 0.6 models at even higher temperature than the ZZ Ceti stars. We have thus selected four DA white dwarfs for which optical and UV data were available to us. These stars are GD 279, GD 64, G210-36, and GD 219. As usual, we fit independently the optical spectra and the UV spectra for various versions of the MLT and compare the derived temperatures in Figure 15. For each version of the

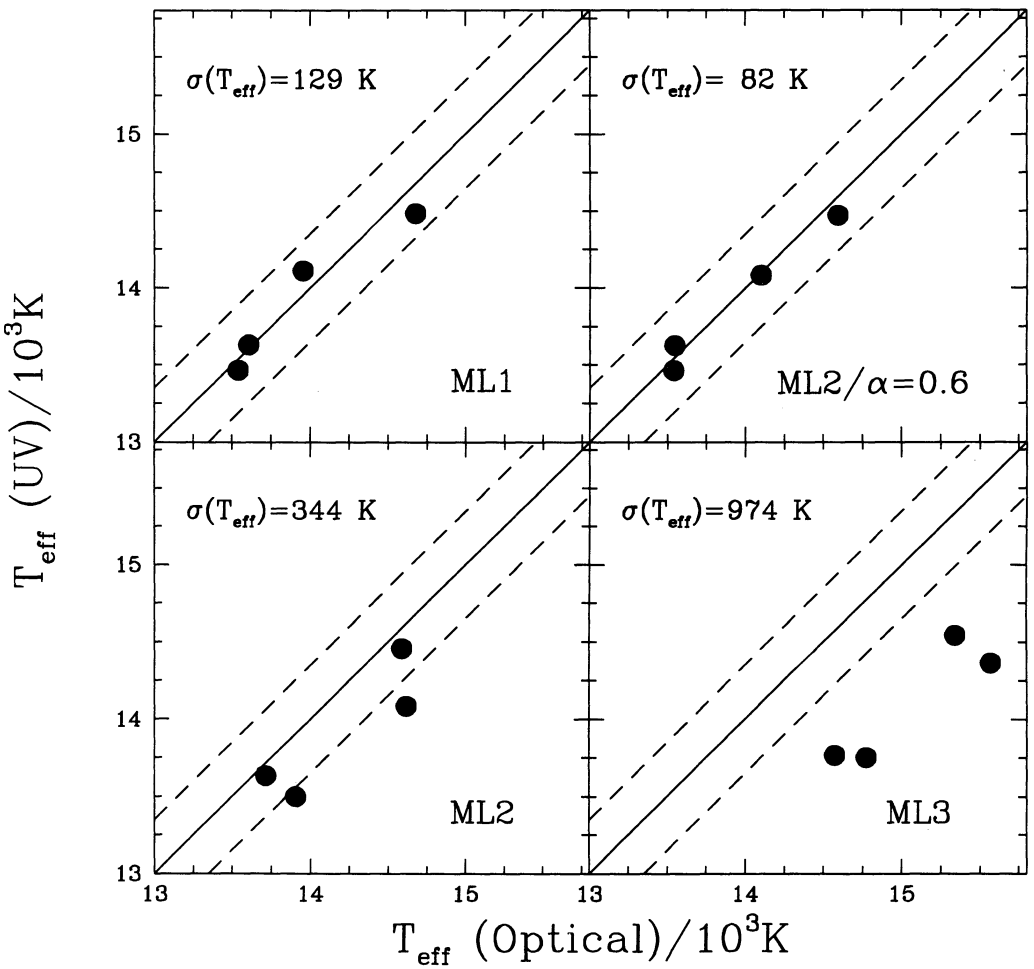

FIG. 15.—Comparison of the effective temperatures derived from UV spectra with those obtained from the optical spectra for four DA stars above the blue edge of the ZZ Ceti instability strip, and for various parameterizations of the MLT. The solid lines indicate the locus where $T_{\rm eff}$(optical) = $T_{\rm eff}$(UV), while the dashed lines represent the $\pm$350 K uncertainty allowed by the optical analysis. In each panel, the value of the standard deviation between both sets of temperatures is indicated.

MLT, we also give the standard deviation between the temperature estimates. Our results indicate that the ML2/α = 0.6 models provide the best internal consistency for hotter DA stars as well. ML1 models also yield a satisfactory agreement, while the optical temperatures derived with ML2 or ML3 models are significantly hotter than those obtained from UV data. The results indicate that such hot DA stars have atmospheres which are only marginally convective.

Our best fits to the UV spectra of these four DA stars with the ML2/α = 0.6 models are illustrated in Figure 16. In contrast to the ZZ Ceti stars shown in Figure 12, these hot DA stars do not exhibit the 1600 Å feature, while the 1400 Å is much stronger here. The excellent quality of the fits to the observed 1400 Å feature strengthens our confidence in the new calculations of Allard et al. (1994). Furthermore, at least two of these stars have surface gravities which are more representative of the DA stars analyzed by BSL. Indeed, GD 279 (log g = 7.83) and GD 64 (log g = 7.73) are less massive than any of the ZZ Ceti stars in Table 4. This shows, at least, that our models do not systematically yield higher surface gravities than the average mean for DA stars. We thus conclude that the ML2/α = 0.6 provides a good description of the emergent fluxes in this range of temperature as well.

4.4. *Hydrodynamical Simulations of Convection in DA Stars*

The mixing-length theory is by far the most commonly used theory used in model atmosphere calculations. Not only did it remain the only theory available in the literature for many years, but the MLT has the advantage of being easily implemented in model atmosphere codes. Recently, alternative theories have been proposed (see, e.g., Canuto & Mazzitelli 1991, 1992; Lydon, Fox, & Sofia 1992, 1993; Grossman, Narayan, & Arnett 1993). Similarly, convective energy transport has also been studied from detailed numerical simulations (see for instance Grossman & Narayan 1993; Ludwig et al. 1994). The study of Ludwig et al. is of particular interest in the present context since their numerical simulations were performed in a ZZ Ceti white dwarf model ($T_{\rm eff}$ = 12,600 K, log g = 8.0). They showed, in particular, that the resulting temperature and velocity structures, obtained from a temporal and spatial average of their hydrodynamical simulation, cannot be reproduced with models calculated within the MLT and for a single value of α. Instead the temperature profile at the surface ($\tau_{\rm R} < 0.1$) is bracketed by ML1/α = 1.5 and α = 3.0 models, while in the range $0.1 \lesssim \tau_{\rm R} \lesssim 6$, values of α between 1 and 2 are required. In the much deeper layers, the temperature profile approaches that of α = 4.0 models.

Figure 17 compares the temperature profile of our ML2/α = 0.6 model at $T_{\rm eff}$ = 12,600 K and log g = 8.0 with that obtained from the hydrodynamical calculations of Ludwig et al. We have determined that the Rosseland optical depth where the emergent flux originates ($\tau_\nu \sim \frac{2}{3}$) is located in the range $0.1 \lesssim \tau_{\rm R} \lesssim 2$, excluding the regions where the line cores are formed. This optical depth range is indicated in Figure 17 as

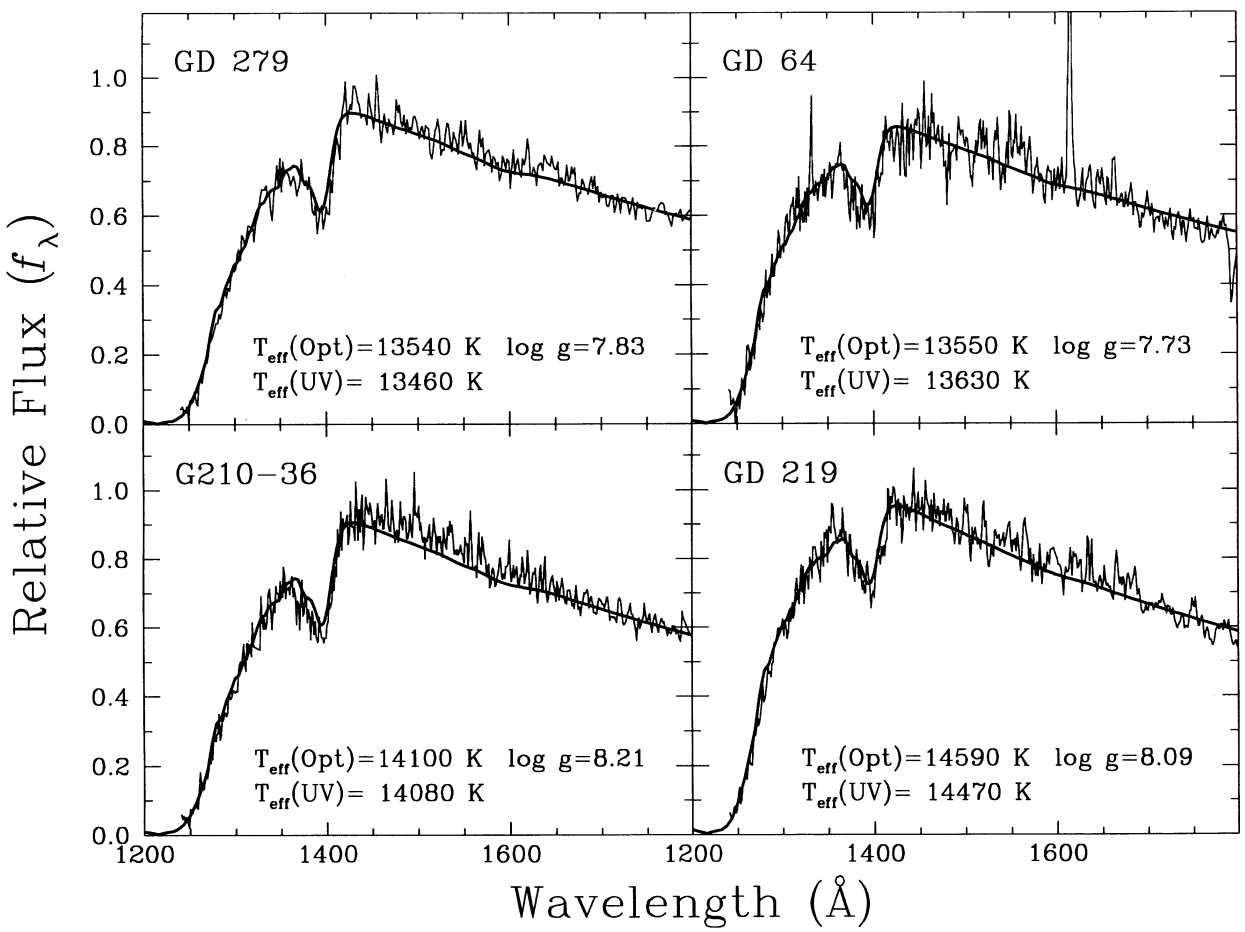

FIG. 16.—Our best fits to the four DA stars discussed in Fig. 15 with ML2/α = 0.6 models; $T_{\rm eff}$ and the solid angle are free parameters in the fitting procedure while log g is taken from the optical determination. UV and optical temperatures are also given for each object.

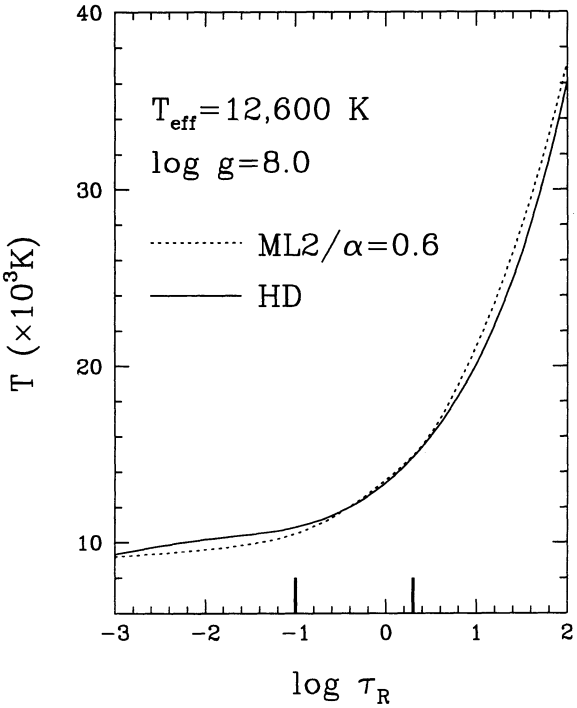

FIG. 17.—Comparison of the temperature profile of the hydrodynamical calculations of Ludwig et al. (1994; *solid line*) with that obtained from our ML2/α = 0.6 model (*dotted line*) at $T_{\rm eff}$ = 12,600 K and log g = 8.0. The range of optical depth where the emergent fluxes originate (with the exception of the line cores) is indicated by heavy tick marks at the bottom.

well. In these layers, the two temperature structures are in very close agreement, especially in the deeper regions where the UV flux originates. For $\tau_R > 1$, however, much larger differences are found. A higher convective efficiency would be required in these regions to match the temperature profile of the hydrodynamical model, in agreement with the conclusions of Ludwig et al. We note that in their calculations, the quasi-molecular features were not included in the opacity calculations, but a comparison of our models where such features are not included indicate that at $T_{\rm eff}$ = 12,600 K, the temperature profiles are not affected significantly by these opacities.

5. CONCLUSIONS

Our analysis of optical and ultraviolet spectrophotometric data of ZZ Ceti stars has demonstrated that it is possible to constrain successfully the convective efficiency in the atmospheres of these stars. Even though recent hydrodynamical calculations indicate that the temperature structure throughout the atmosphere *cannot* be reproduced with model atmospheres calculated within the MLT, our analysis has nevertheless shown that it is still possible with such models to reach an excellent agreement between the temperatures derived from the optical spectroscopy and those obtained from the UV energy distribution, a result which indicates that model atmospheres calculated within the MLT can reproduce reasonably well the temperature profile in those layers where the emergent fluxes originate.

In particular, we found that model atmospheres calculated with ML2/α = 0.6 provide an overall internal consistency between the optical and UV temperature estimates, the observed photometry, the trigonometric parallax measurements, and the gravitational redshift masses. The mean mass of the ZZ Ceti stars derived with such models is somewhat larger by $\sim$0.06 $M_\odot$ than that of hotter DA stars, however. This last result can be explained in most part by the mass dependence of the blue edge of the ZZ Ceti instability strip predicted from recent nonadiabatic calculations, in which the most massive ZZ Ceti stars at the blue edge are hotter than the less massive counterparts. Such a dependence also implies that nonvariable stars should exist within the ZZ Ceti instability strip, in the temperature range defined by the hottest ZZ Ceti star at $T_{\rm eff}$ = 12,460 K, and the coolest one at 11,160 K. However, our analysis has also shown that the identification of such objects requires a detailed and simultaneous analysis of optical and high-quality UV data.

We acknowledge P. Brassard for providing us with unpublished material and for enlightening discussions, and M.-T. Ruiz and S. K. Leggett for their help with the data acquisition of BPM 31594. This work was supported in part by the NSERC Canada, and by the Fund FCAR (Québec).

REFERENCES

Allard, N. F., & Koester, D. 1992, A&A, 258, 464
Allard, N. F., Koester, D., Feautrier, N., & Spielfiedel, A. 1994, A&AS, 108, 417
Bergeron, P. 1993, in White Dwarfs: Advances in Observation and Theory, NATO ASI Series, ed. M. A. Barstow (Dordrecht: Kluwer), 267
Bergeron, P., et al. 1993, AJ, 106, 1987
Bergeron, P., Liebert, J., & Fulbright, M. S. 1995, ApJ, 444, 810
Bergeron, P., Saffer, R. A., & Liebert, J. 1992a, ApJ, 394, 247 (BSL)
Bergeron, P., Saumon, D., & Wesemael, F. 1995, ApJ, 443, 764
Bergeron, P., Wesemael, F., Beauchamp, A., Wood, M. A., Lamontagne, R., Fontaine, G., & Liebert, J. 1994, ApJ, 432, 305
Bergeron, P., Wesemael, F., & Fontaine, G. 1991, ApJ, 367, 253
———. 1992b, ApJ, 387, 288
Bergeron, P., Wesemael, F., Fontaine, G., & Liebert, J. 1990, ApJ, 351, L21
Böhm, K.-H., & Cassinelli, J. P. 1971, A&A, 12, 21
Böhm-Vitense, E. 1958, ZsAp, 46, 108
Bradley, P. A., & Winget, D. E. 1991, ApJS, 75, 463
———. 1994a, ApJ, 421, 236
———. 1994b, ApJ, 430, 850
Bragaglia, A., Renzini, A., & Bergeron, P. 1995, ApJ, 443, 735
Brassard, P., et al. 1995a, in preparation
Brassard, P., Fontaine, G., & Wesemael, F. 1995b, ApJS, 96, 545
Brassard, P., Fontaine, G., Wesemael, F., & Hansen, C. J. 1992a, ApJS, 80, 369
Brassard, P., Fontaine, G., Wesemael, F., Kawaler, S. D., & Tassoul, M. 1991, ApJ, 367, 601
Brassard, P., Fontaine, G., Wesemael, F., & Talon, A. 1993, in White Dwarfs: Advances in Observation and Theory, NATO ASI Series, ed. M. A. Barstow (Dordrecht: Kluwer), 485
Brassard, P., Fontaine, G., Wesemael, F., & Tassoul, M. 1992b, ApJS, 81, 747
Brassard, P., Pelletier, C., Fontaine, G., & Wesemael, F. 1992c, ApJS, 80, 725
Brickhill, A. J. 1991, MNRAS, 252, 334
———. 1992a, MNRAS, 259, 519
———. 1992b, MNRAS, 259, 529
Canuto, V. M., & Mazzitelli, I. 1991, ApJ, 370, 295
———. 1992, ApJ, 389, 724
Dahn, C., & Harrington, R. 1991, private communication
Daou, D., Wesemael, F., Bergeron, P., Fontaine, G., & Holberg, J. B. 1990, ApJ, 364, 242
Fontaine, G., Bergeron, P., Lacombe, P., Lamontagne, R., & Talon, A. 1985, AJ, 90, 1094
Fontaine, G., Bergeron, P., Vauclair, G., Brassard, P., Wesemael, F., Kawaler, S. D., Grauer, A. D., & Winget, D. E. 1991, ApJ, 378, L49
Fontaine, G., Brassard, P., Bergeron, P., & Wesemael, F. 1992, ApJ, 399, L91
Fontaine, G., Brassard, P., Wesemael, F., & Tassoul, M. 1994, ApJ, 428, L61
Fontaine, G., McGraw, J. T., Dearborn, D. S. P., Gustafson, J., & Lacombe, P. 1982, ApJ, 258, 651
Fontaine, G., Tassoul, M., & Wesemael, F. 1984, in Proc. 25th Liège Astrophysical Colloq., Theoretical Problems in Stellar Stability and Oscillations, ed. A. Noels & M. Gabriel (Liège: Université de Liège), 328

Fontaine, G., Villeneuve, B., & Wilson, J. 1981, ApJ, 243, 550
Fontaine, G., & Wesemael, F. 1991, in IAU Symp. 145, Evolution of Stars: The Stellar Abundance Connection; ed. G. Michaud & A. Tutukov (Dordrecht: Reidel), 421
Greenstein, J. L. 1982, ApJ, 258, 661
Grossman, S. A., & Narayan, R. 1993, ApJS, 89, 361
Grossman, S. A., Narayan, R., & Arnett, D. 1993, ApJ, 407, 284
Hammond, G. L., Sion, E. M., Kenyon, S. J., & Aannestad, P. A. 1991, in Proc. 7th European Workshop on White Dwarfs, NATO ASI Series, ed. G. Vauclair & E. M. Sion (Dordrecht: Kluwer), 317
Heber, U., Hunger, K., Jonas, G., & Kudritzki, R. P. 1984, A&A., 130, 119
Hummer, D. G., & Mihalas, D. 1988, ApJ, 331, 794
Kawaler, S. D., & Bradley, P. A. 1994, ApJ, 427, 415
Kawaler, S. D., et al. 1995, preprint
Kawaler, S. D., & Hansen, C. J. 1989, in IAU Colloq. 114, White Dwarfs, ed. G. Wegner (New York: Springer), 97
Kepler, S. O., & Nelan, E. P. 1993, AJ, 105, 608
Koester, D. 1991, in Proc. 7th European Workshop on White Dwarfs, NATO ASI Ser., ed. G. Vauclair & E. M. Sion (Dordrecht: Kluwer), 343
Koester, D., & Allard, N. 1993, in White Dwarfs: Advances in Observation and Theory, NATO ASI Ser., ed. M. A. Barstow (Dordrecht: Kluwer), 237
Koester, D., Allard, N. F., & Vauclair, G. 1994, A&A, 291, L9
Koester, D., Weidemann, V., Zeidler-K. T., E.-M., & Vauclair, G. 1985, A&A, 142, L5
Lamontagne, R., Wesemael, F., & Fontaine, G. 1987, in IAU Colloq. 95, Proc. 2d Conf. on Faint Blue Stars, ed. A. G. Davis Philip, D. S. Hayes, & J. Liebert (Schenectady: L. Davis), 677
Lamontagne, R., Wesemael, F., Fontaine, G., Wegner, G., & Nelan, E. P. 1989, in IAU Colloq. 114, White Dwarfs, ed. G. Wegner (New York: Springer), 240
Lenzuni, P., Chernoff, D. F., & Salpeter, E. E. 1991, ApJS, 76, 759
Ludwig, H.-G., Jordan, S., & Steffen, M. 1994, A&A, 284, 105
Lydon, T. J., Fox, P. A., & Sofia, S. 1992, ApJ, 397, 701
———. 1993, ApJ, 403, L79
McGraw, J. T. 1977, Ph.D. thesis, Univ. of Texas at Austin
———. 1979, ApJ, 229, 203
Nather, R. E. 1989, in IAU Colloq. 114, White Dwarfs, ed. G. Wegner (New York: Springer), 109
Nather, R. E., Winget, D. E., Clemens, J. C., Hansen, C. J., & Hine, B. P. 1990, ApJ, 361, 309
Nelan, E. P., & Wegner, G. 1985, ApJ, 289, L31
Olson, E. C. 1974, PASP, 86, 80
Press, W. H., Flannery, B. P., Teukolsky, S. A., & Vetterling, W. T. 1986, Numerical Recipes (Cambridge: Cambridge Univ. Press)
Robinson, E. L. 1979, in IAU Colloq. 53, White Dwarfs and Variable Degenerate Stars, ed. H. M. Van Horn & V. Weidemann (Rochester: Univ. of Rochester Press), 343
Saffer, R. A., Bergeron, P., Koester, D., & Liebert, J. 1994, ApJ, 432, 351
Saffer, R. A., Liebert, J., & Olszewski, E. M. 1988, ApJ, 334, 947
Schulz, H. 1978, A&A, 68, 75
Seaton, M. J. 1990, J. Phys. B, 23, 3255
Tassoul, M., Fontaine, G., & Winget, D. E. 1990, ApJS, 72, 335
van Altena, W. F., Lee, J. T., & Hoffleit, E. D. 1994, The General Catalogue of Trigonometric Parallaxes (New Haven: Yale Univ. Obs.)
Van Horn, H. M. 1984, in Proc. 25th Liège Astrophysical Colloq., Theoretical Problems in Stellar Stability and Oscillations, ed. A. Noels & M. Gabriel (Liège: Univ. de Liège), 307
Weidemann, V., & Koester, D. 1984, A&A, 132, 195
Wegner, G., & Reid, I. N. 1991, AJ, 375, 674
Wesemael, F., Auer, L. H., Van Horn, H. M., & Savedoff, M. P. 1980, ApJS, 43, 159
Wesemael, F., Bergeron, P., Fontaine, G., & Lamontagne, R. 1991, in Proc. 7th European Workshop on White Dwarfs, NATO ASI Ser., ed. G. Vauclair & E. M. Sion (Dordrecht: Kluwer), 159
Wesemael, F., Lamontagne, R., & Fontaine, G. 1986, AJ, 91, 1376
Winget, D. E. 1988, in IAU Symp. 123, Advances in Helio- and Asteroseismology, ed. J. Christensen-Dalsgaard & S. Frandsen (Dordrecht: Reidel), 305
———. 1991, in Proc. 7th European Workshop on White Dwarfs, ed. G. Vauclair & E. M. Sion (Dordrecht: Kluwer), 159
Winget, D. E., et al. 1991, ApJ, 378, 326
———. 1994, ApJ, 430, 839
Winget, D. E., & Fontaine, G. 1982, in Pulsations in Classical and Cataclysmic Variable Stars, ed. J. P. Cox & C. J. Hansen (Boulder: Univ. of Colorado), 46
Wood, M. A. 1990, Ph.D. thesis, Univ. of Texas at Austin
———. 1995, in Proc. 9th European Workshop on White Dwarfs, NATO ASI Series, ed. D. Koester & K. Werner (Berlin: Springer), in press
Zuckerman, B., & Becklin, E. E. 1992, ApJ, 386, 260